catalysts

MDPI

Review

Hydroisomerization Catalysts for High-Quality Diesel Fuel Production

Yamen Aljajan [1,2], Valentin Stytsenko [1], Maria Rubtsova [1] and Aleksandr Glotov [1,*]

[1] Physical and Colloidal Chemistry Department, Faculty of Chemical Technology and Ecology, Gubkin University, 119991 Moscow, Russia; aljajan@gubkin.ru or yamen.jajan@alfuratuniv.edu.sy (Y.A.); vds41@mail.ru (V.S.); rubtsova.m@gubkin.ru (M.R.)

[2] Petro-Processes Engineering Department, Faculty of Petrochemical Engineering, Alfurat University, Deir ez-Zur 84C7+XHV, Syria

* Correspondence: glotov.a@gubkin.ru

Abstract: Upgrading the properties of diesel fractions is considered one of the crucial processes in the petrochemical industry; and for this purpose in laboratory-scale researching it is studied on the base of the hydroisomerization of n-hexadecane as a main model reaction. Recently, zeolite-based bifunctional catalysts have proven their efficiency due to their remarkable acidity, shape-selectivity and relative resistance to deactivation. In this review, different topological-type zeolite-based catalysts, the mechanism of their catalytic effect in n-C_{16} isomerization, and the principles of shape-selectivity are reviewed. A comparison of their structural-operational characteristics is made. The impact of some feedstock impurities on the catalyst's performance and deactivation due to carbonaceous deposits as well as various modern eco-friendly cost-effective synthesis techniques are also discussed.

Keywords: hydroisomerization; hydrocracking; zeolite-based catalysts; hexadecane; shape selectivity

check for updates

Citation: Aljajan, Y.; Stytsenko, V.; Rubtsova, M.; Glotov, A. Hydroisomerization Catalysts for High-Quality Diesel Fuel Production. *Catalysts* **2023**, *13*, 1363. https://doi.org/10.3390/catal13101363

Academic Editor: Valeria La Parola

Received: 19 September 2023
Revised: 5 October 2023
Accepted: 9 October 2023
Published: 11 October 2023

1. Introduction

Currently, a key focus in the global production of petroleum products is to raise the standards for motor fuels. The inadequate quality of such fuels is a leading factor contributing to environmental pollution. To address this issue, improving the chemical composition of the fuel is used to meet high quality requirements [1,2]. One of the most promising technologies is isodewaxing process. Instead of removing n-paraffins by solvent extraction, the is the odewaxing technology modifies the molecular structure of the wax through catalytic isomerization, producing isoparaffins with superior cold flow properties, high viscosity index, and excellent oxidation resistance.

The isodewaxing process comprises four reactions: (i) isomerization of the normal paraffins to obtain their isomers, (ii) hydrocracking of the long-chain paraffins into shorter-chain ones, (iii) hydrogenation of the unsaturated aromatic components, and (iv) hydrodecyclization with the ring-opening reaction. In this review we will focus on the first type of reaction, which usually occurs in the presence of hydrogen, so it is referred to as hydroisomerization. Usually, this reaction is accompanied by hydrocracking in which the extent varies according to the operational conditions of the process and the characteristics of the catalyst used. The rates of hydroisomerization and hydrocracking reactions define the composition of products.

Considerable research efforts have been dedicated towards the production of value-added products from low-grade waxy feedstocks (Figure 1). In particular, the focus has been on converting these feedstocks into branched products to improve the fuel quality. These researches have been centered on catalysts development, with a specific emphasis on micro/mesoporous catalysts to accelerate mass transfer and optimize the residence time of reagents on the active sites, thereby increasing their efficiency in the desired chemical reactions [3–6].

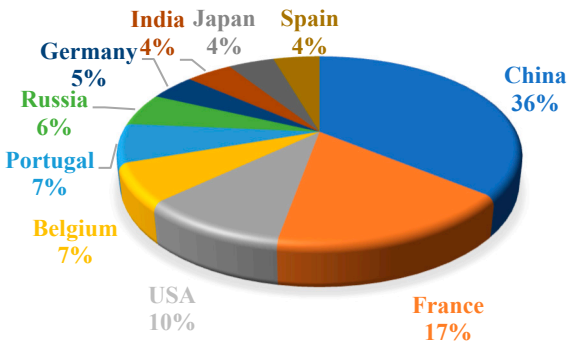

Figure 1. Distribution of published papers on isomerization of n-C_{16} paraffins by countries [sourced from Scopus database].

Hydroisomerization catalysts are generally categorized as bifunctional catalysts, composed of a metal, typically platinum, that is dispersed on an acidic support. The metal serves as a dehydrogenation/hydrogenation agent, while the acidic support aids in the skeletal isomerization reaction of the olefinic intermediates created over the metal sites and in cracking [7,8]. A well-balanced bifunctional catalyst promotes hydrogenation and dehydrogenation reactions, with rearrangements of the hydrocarbon intermediates over acid sites dictating reaction rates [9]. As a result, hydroisomerization and hydrocracking reactions occur in sequence, leading to mono- and multibranched isomers, and cracked paraffins [10,11]. One of the primary challenges in advancing the hydroisomerization technology is the need for highly effective and selective bifunctional catalysts that can minimize the formation of byproducts resulting from hydrocracking [12,13].

In this review, the latest findings in improving the isomerization processes of linear alkanes through the development of catalyst structures, methods of their preparation, and studies related to the operational conditions of the process will be discussed. A comprehensive analysis will be conducted to compare the performance of various catalysts during the hydroisomerization of n-C_{16}. The operating conditions of the hydroisomerization of n-C_{16} will be discussed in details.

2. Straight-Chain Alkane Hydroisomerization Process

2.1. The Principle of the Process and Its Technical Significance

Hydroisomerization of diesel fraction is considered as a vital chemical process that includes the hydroconversion of normal paraffins into their branched isomers. This reaction comprises breaking and rearranging C-C bonds to obtain more favorable isomers providing the higher cetane number of diesel, thus reducing engine emissions and improving the cold flow characteristics of fuels, making them less prone to clogging at low temperatures.

As shown in Table 2, the presence of linear alkanes improves the cetane number of diesel, however, the melting point also increases. Given the importance of diesel quality, maintaining an adequate cetane number is crucial. According to the 2019 Worldwide Fuel Charter, the minimum cetane number equals 51.0 and up to 55.0 for some markets having high requirements for emission control [14].

It should be noted that branched-chain paraffins typically have lower cetane numbers than their linear counterparts. Among the mono-branched isomers with alkyl substituents or with methyl groups at the end of the hydrocarbon chain, the latter not only have lower melting points but also higher cetane numbers (Table 1). Therefore, the selective hydroisomerizing n-alkanes to these isomers can produce diesel with improved cold flow properties and a shorter ignition delay [15].

Table 1. Characteristics of hexadecane isomers as a fuel component [PubChem database]; [16].

Isomer	Chemical Structure	Boiling Point [a], °C	Flash Point [a], °C	Melting Point [a], °C	Cetane Number
Mono-isomers 2-methylpentadecane	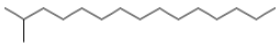	282.0	95.3	−9.2	100
8-methylpentadecane	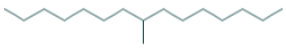	274.3	94.0	−25.6	75
5-butyldodecane	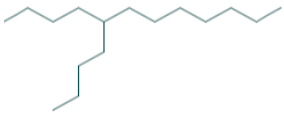	150.7 [b]	N/A	−47.4	45
Di-isomers (3R,4R)-dimethyltetradecane (3R,4S)-dimethyltetradecane (3S,4R)-dimethyltetradecane (3S,4S)-dimethyltetradecane	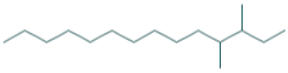	248.0	N/A	−37.0	61 64 58 62
(5R,6R)-dimethyltetradecane (5R,6S)-dimethyltetradecane (5S,6R)-dimethyltetradecane (5S,6S)-dimethyltetradecane	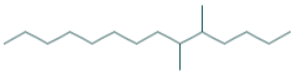	N/A	N/A	N/A	51 51 48 52
7,8-dimethyltetradecane	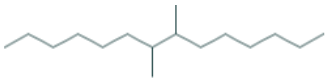	270.0	−86.2	−86.2	40
Multi-branched isomers 2,2,4,4,6,8,8-heptamethylnonane	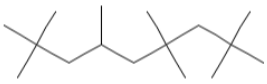	247.0	102.0	N/A	15

[a] Measured at 750 mmHg. [b] Measured at 20 mmHg.

Table 2. Characteristics of n-alkanes C_3-C_{18} as a fuel component (sourced from PubChem database [16]).

Alkane	Chemical Formula	Boiling Point (°C)	Melting Point (°C)	Flash Point (°C)	Cetane Number
n-propane	C_3H_8	−42.0	−187.6	−104.0	−20.0
n-butane	C_4H_{10}	0.5	−138.3	−60.0	20.6
n-pentane	C_5H_{12}	36.0	−129.0	−40.0	30.0
n-hexane	C_6H_{14}	69.0	−95.4	−22.0	47.9
n-heptane	C_7H_{16}	98.4	−90.6	−4.0	56.0
n-octane	C_8H_{18}	125.6	−56.7	13.0	64.4
n-nonane	C_9H_{20}	150.5	−53.5	31.0	60.9
n-decane	$C_{10}H_{22}$	174.1	−29.7	46.0	65.5
n-undecane	$C_{11}H_{24}$	195.9	−25.5	62.0	79.0
n-dodecane	$C_{12}H_{26}$	216.3	−9.6	83.0	72.9
n-tridecane	$C_{13}H_{28}$	235.4	−5.4	94.0	88.0
n-tetradecane	$C_{14}H_{30}$	253.6	5.9	100.0	95.0
n-pentadecane	$C_{15}H_{32}$	270.6	10.0	N/A	98.0
n-hexadecane	$C_{16}H_{34}$	286.9	18.2	135.0	100.0
n-heptadecane	$C_{17}H_{36}$	303.0	22.0	149.0	105.0
n-octadecane	$C_{18}H_{38}$	316.0	28.2	166.0	110.0

From a thermodynamic point of view, the formation of iso-paraffins is more favorable at lower temperatures; therefore, to achieve better selectivity towards isomers, catalysts are usually designed for low temperature exploitation [17,18].

2.2. Illuminating the Pathways of Molecular Transformation

Zeolites composed entirely of silica have a neutral charge, however, if Si^{4+} is replaced with Al^{3+}, the framework becomes negatively charged. Protons can neutralize the framework charges, resulting in the development of acid sites that accelerate the main processes of oil refining: hydrocarbon isomerization and cracking. Based on the zeolite topology and acidity, these processes can yield desirable products by converting linear alkanes into diverse branching isomers and breaking down higher hydrocarbons into smaller ones [19]. Before digging into the influence of shape selectivity on these reactions, it is crucial to look at the case where shape selectivity is omitted.

Conventional hydroisomerization proceeds with the formation of an olefinic intermediate via dehydrogenation on the metal site. As a result of the highly endothermic nature of the dehydrogenation step, the concentration of olefins in the hydroisomerization reaction mixture is typically low. Thus, it is crucial to convert these olefinic compounds promptly to carbocations on the acid sites of the catalyst to ensure efficient conversion. Due to the weak basicity of the hydrocarbons, the equilibrium concentration of carbocations on the acid sites of the zeolite is relatively low [20,21].

According to Jacob et al. [22], there are two types of carbocations:

- Tricoordinated carbenium ion;
- Pentacoordinated carbonium ion (extremely unstable).

Carbenium ions can be formed via three distinct routes depending on feedstock properties and the catalyst acidity. These routes include (i) hydride elimination on Lewis acid sites (Figure 2a), which can occur through a variant pathway of the carbenium ion R^+ adsorbed on active sites of the zeolite, known as "bimolecular hydride transfer" (Figure 2b); (ii) alkane protonation followed by hydrogen abstraction (Figure 2c); and (iii) olefin protonation, leading to the formation of an alkylcarbenium ion (Figure 2d). The last route comprises the protonation of olefinic intermediates instead of the energetically unfavorable direct protonation of alkanes. Thus, the isomerization via route (iii) accelerates as compared to the direct activation of the alkanes [22].

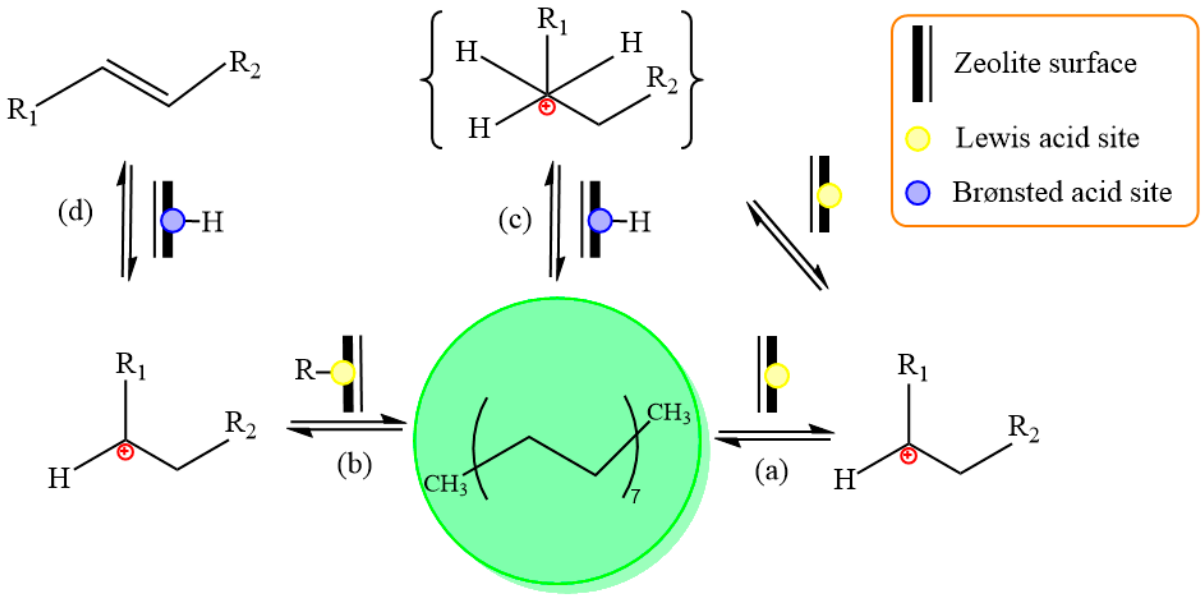

Figure 2. Routes of carbenium ions formation. (**a**) hydride elimination at Lewis type acid sites, (**b**) hydride elimination on adsorbed carbenium ion, (**c**) alkane protonation, and (**d**) olefin protonation.

As per the classical bifunctional mechanism of the isomerization, the metal component of the catalyst facilitates the dehydrogenation of alkanes to form alkenes that are protonated to transitional alkylcarbenium ions on the Brønsted acid sites. These ions undergo rearrangement and scission reactions to obtain ultimately obtain, after hydrogenation on the

metal sites, the saturated product—mono-substituted isoalkanes. In the case of availability of potent Brønsted acid sites, mono-substituted tertiary carbenium ions may undergo additional isomerization, finally leading to the formation of carbenium ions containing multi-branches [23].

Aluminosilicate zeolites that incorporate platinum or palladium metal typically operate based on the classical bifunctional mechanism (Figure 3), particularly at high conversions, elevated hydrogen pressure, and a sufficiently high carbon number of the feedstock. The pathway of converting hydrocarbons on metals often compete with the bifunctional mechanism, and the significance of the former increases in the case of more severe conditions and the weak acidity of zeolite. The presence of CH_4 and C_2H_6 in the final reaction products is indicative of metal-catalyzed cracking, a process commonly referred to as hydrogenolysis.

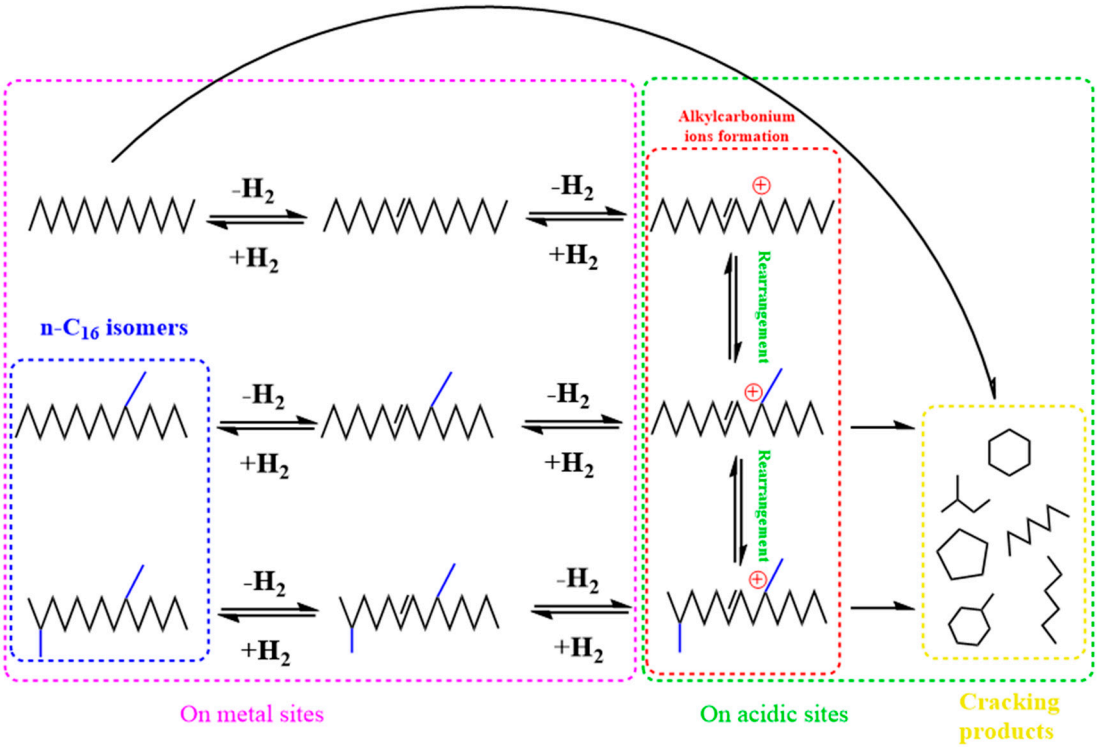

Figure 3. Mechanism of hydroisomerization of n-hexadecane.

Weiss demonstrated that alkenes displayed high reactivity in the isomerization on Pt-free aluminosilicate, whereas alkanes did not [24]. Several studies have reported an increase in the isomerization rate with rising Pt content, which can be attributed to high concentration of the olefinic intermediate [25,26].

Due to the formation of strong covalent bonds, both the enthalpy of protonation (ΔH_p) and the activation energy of the isomerization step (E_{iso}) are expected to be high, as a result of the deformation of the C-O-Z bond (Z-acid site). The skeletal isomerization reaction is postulated to occur through the rearrangement of the carbenium ion via a cycloalkyl intermediate. The resulting isoparaffinic carbenium ion is subsequently transformed into an olefin via the loss of proton at the acid site. Finally, the isoolefin intermediate is rapidly hydrogenated to the isoalkane product [27].

The rate of isomerization has been observed to be heavily influenced by the length of the alkane chain. The longer chains result in the greater stability of bound carbenium ions and the higher rate of the isomerization reaction. However, high isomerization selectivity becomes increasingly challenging as the chain length increase, due to adverse reactions, namely carbocation intermediate hydrocracking on acid sites and hydrogenolysis reactions on metal sites. The balance between hydrogenation and acid function is a key factor that

governs the prevalence of acid- or metal-catalyzed reactions, ultimately determining the composition of products [28,29].

Three mechanisms of alkane cracking have been established: (a) non-catalytic thermal cracking that proceeds at high temperatures as radical process, (b) proteolytic α-cracking including carbonium ion and (c) β-cracking via the carbenium ion. The commonly acknowledged mechanisms of catalytic cracking in hydroisomerization conditions can be described using two fundamental steps: the formation of carbenium ions and β-cracking.

In contrast to acid-catalyzed cracking, the product of thermal cracking of alkanes via free-radical intermediates possesses a the distinct composition (Table 3).

Table 3. Comparison of thermal and catalytic cracking processes.

Hydrocarbons	Thermal Cracking Products	Catalytic Cracking Products
n-Hexadecane	Primary products—alkanes C_1-C_3; significant quantity of n-olefins C_4-C_{15}; relatively low concentrations of branched aliphatics	Primary products—alkanes C_3-C_6; minor amounts of n-olefins; high concentrations of branched aliphatics
Aliphatics	Minor conversion to aromatics at 500 °C	Large conversion to aromatics at 500 °C
n-olefins	Slow sigmatropic rearrangement of double bond with a low isomerization	Rapid sigmatropic rearrangement of double bond with a significant isomerization conversion
Branched olefins	Non-selective hydrogen transfer and lower rate of cracking as compared to that of the corresponding alkanes	Selective hydrogen transfer and higher rate of cracking than that of the corresponding alkanes
Naphthenes	The rate of cracking is lower than that of the corresponding alkanes.	The rate of cracking is comparable to that of the corresponding alkanes.
Alkyl aromatics	Cracking happens within the side of alkyl functional groups	Cracking happens within the side of aromatic ring itself
Alkyl aromatics with larger functional groups	The rate of cracking is lower than that of the corresponding alkanes	The rate of cracking is higher than that of the corresponding alkanes

Typically, the formation of free-radical intermediates in the process is of kinetic significance at temperatures higher than 530 °C [30,31].

According to the traditional catalytic cracking mechanism (also known as the carbenium ion mechanism), an alkane is subjected to hydride abstraction by a carbenium ion, resulting in the formation of another carbenium ion, which then undergoes β-scission, or the cleavage of the C-C bond β-situated to the trivalent carbocation [32]. Carbenium ions are known to act as chain carriers, with the most stable ones, typically tertiary ions like the t-butyl cation, being the predominant carriers [33,34].

3. n-Hexadecane Hydroisomerization on Bifunctional Catalysts

3.1. Development of Hydroisomerization Catalysts

To improve the formation and isomerization of the carbocation intermediate in the hydroisomerization reaction, the catalyst must have a significant acidity [35,36]. Since the discovery of aluminum chloride in 1933 as a catalyst for hexane and heptane isomerization, four generations of hydroisomerization catalysts have been developed over the course of several decades (Table 4) [37–39]. Currently, only third and fourth generations are used in the industry, although the academic interest in these generations of catalysts has increased dramatically over the past 10 years (Figure 4), and this review focuses on the last generation. A critical challenge in the research and development of innovative hydroisomerization catalysts is to achieve high selectivity of isomerization and considerable n-paraffin conversion, constraining the formation of cracking byproducts. This parallel reaction reduces the yield of the intended products [40].

Table 4. Catalysts generations for hydroisomerization of n-alkanes.

Generation	Catalysts Composition	Operating Temperature, °C	Advantages	Disadvantages
1st	Friedel-Crafts, $AlCl_3$	80–100	High activity	Sensitivity to trace water; fast deactivation
2nd	Metal/support	350–500	Easy to apply; corrosion issues are mitigated; sensitivity problems are less severe	Thermodynamic limitations on conversion
3rd	Metal/halogenated support	120–160	Enhanced acidity due to halogenation (Cl, F) of alumina support	Sensitive to impurities; continuous feeding chlorine to maintain catalyst activity; corrosion of equipment
4th	Bifunctional zeolite-based catalysts	250–340	Easy to use; tolerant to poisons; no feedstock pretreatment	Selectivity issues; more expensive to produce

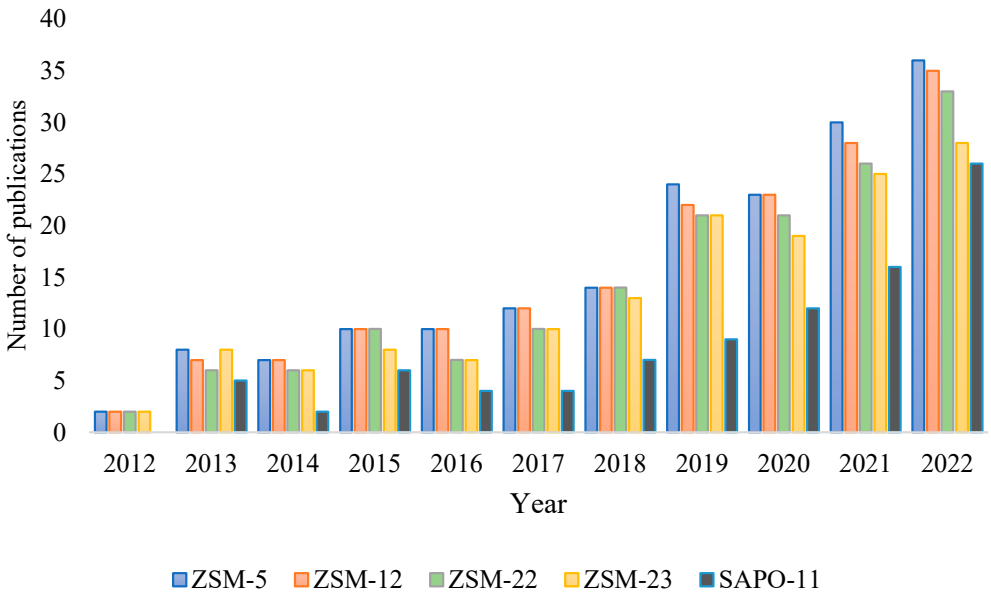

Figure 4. The study of n-alkanes isomerization on zeolite-based catalysts over the last decade [ScienceDirect database].

Typical zeolites-based catalysts are prone to poisoning and deactivation in the hydroisomerization process of linear alkanes due to the presence of sulfur-containing substances in the feed. Currently, the major developments in the design of catalysts for n-paraffin hydroisomerization are the high efficiency at temperatures 100–200 °C and tolerance to both sulfur and water.

Synthetic zeolites have been recognized as solid acid catalysts and are widely used in a variety of applications in industry, notably in petrochemical synthesis and oil refining [41]. The topology and morphology of the zeolites defines their suitability for the particular application process (Table 5), which is defined by interlinked channel structures or a hierarchical structure that integrates micro- and mesopores, in addition to acid-base properties [42–46].

Table 5. The standard structural properties of zeolites [Database of Zeolite Structure].

Zeolite	Topology	Member Ring (MR)	Channel Dimensionality	Accessible Volume, %
ZSM-5	MFI	10, 6, 5, 4	3D	9.81
ZSM-12	MTW	12, 6, 5, 4	1D	9.42
ZSM-22	TON	10, 6, 5	1D	8.04
ZSM-23	MTT	10, 6, 5	1D	7.98
ZSM-35	FER	10, 8, 6, 5	2D	10.01
ZSM-48	MRE	10, 6, 5, 4	1D	6.55
SAPO-11	AEL	10, 6, 4	1D	6.77
Beta	BEA	12, 6, 5, 4	3D	20.52
Mordenite	MOR	12, 8, 5, 4	2D	12.27
EMM-23	EWT	21, 10, 6, 5, 4	3D	21.95

3.2. Analysis of the Relationship between Catalyst Characteristics and Activity

3.2.1. Shape-Selectivity

The study of the structural effect of zeolites on their selectivity deals with the concept of "shape-selectivity" that is classified into two basic categories: configurational selectivity and transition state selectivity (Figure 5). Typically, zeolites acquire the requisite shape selectivity at the expense of restricted mass transfer inside micropores to and from the active sites. To overcome this issue, several approaches have been used to improve the accessibility of active sites inside zeolites. One successful way is to take advantage of molecular shape selectivity, which acts inside zeolite' channel systems and has shown higher efficiency and selectivity in various chemical reactions.

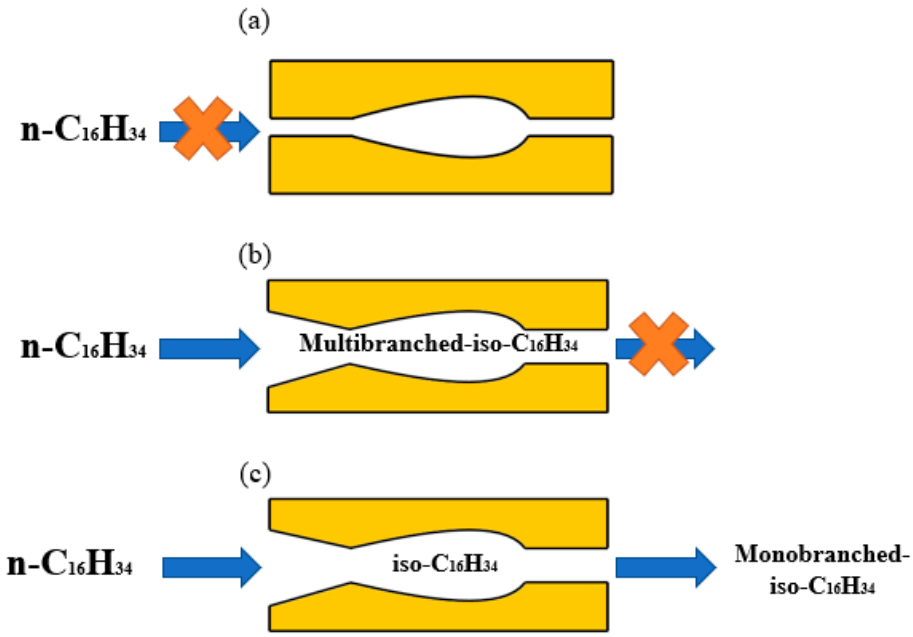

Figure 5. Representation of basic shape selectivity types in the zeolite: (**a**) reactant shape selectivity; (**b**) transitional-state shape selectivity; (**c**) product shape selectivity.

Configurational selectivity arose from the insight that molecule cannot pass through the channels of the zeolite. In the case where the molecule will not be adsorbed it will keep staying intact in the resultant mixtures (reactant shape selectivity) (Figure 5a). In the case where the molecule will not be desorbed, it can exist as an adsorption transitional-state, and

only molecules originating from this state will be included in the product via the following reactions (product shape selectivity) (Figure 5b). In addition, the effective pore diameter may strongly affect the formation of transition-state intermediates and direct them towards forming states that fit its topology or towards participating in secondary intermediate interactions (transitional-state shape selectivity) (Figure 5c).

In some cases, transition state intermediates approximating the topological framework of the zeolite are quickly formed (inverse shape selectivity) (Figure 6a), this phenomenon was caused by sorption shape selectivity instead of transition state shape selectivity, as previously thought [47,48].

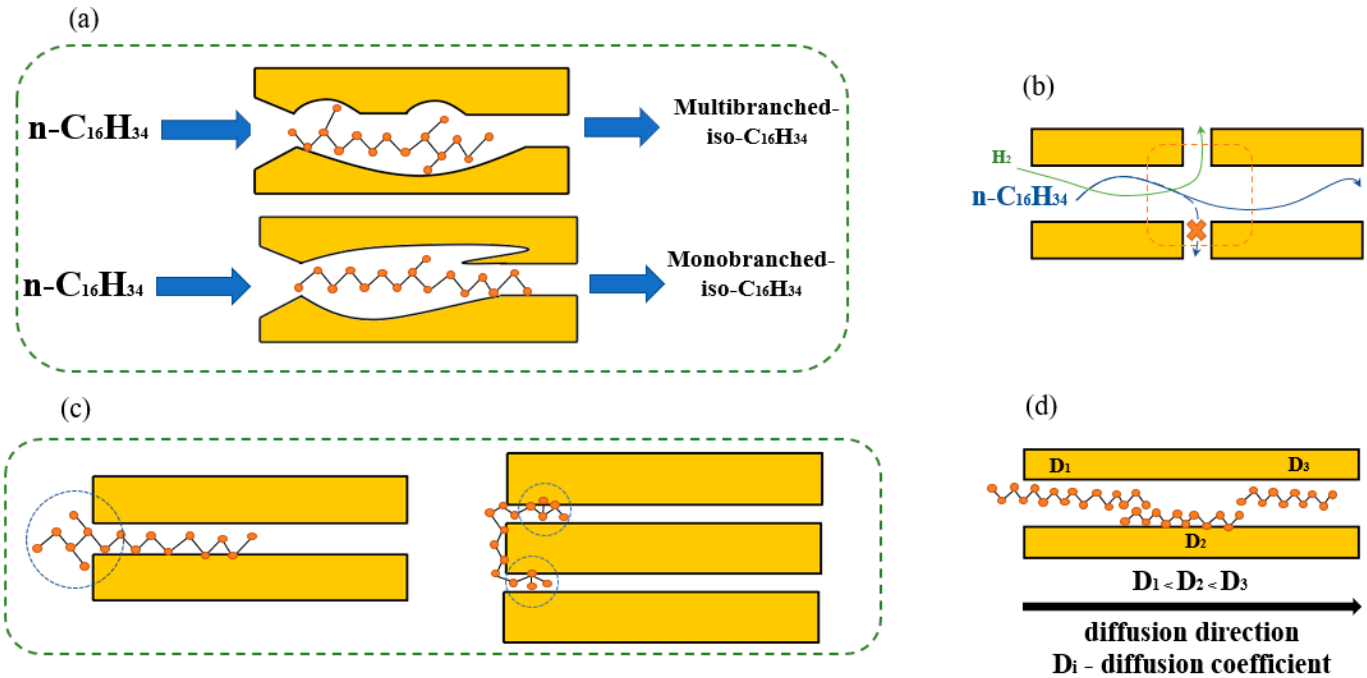

Figure 6. Representation of secondary shape selectivity types in the zeolite: (**a**) inverse shape selectivity; (**b**) molecular traffic shape selectivity; (**c**) pore mouth and key-lock selectivity; (**d**) the window effect.

Transition state selectivity can be influenced by restrictions that could occur either on the surface or within the pores of the framework of the zeolite. In the locations where the paths of the pores happen to intersect, this case can affect the diffusion of the reactant molecules—whether due to geometric reasons or the characteristics of molecular diffusion. As a result, molecules of the specific reactant may enter one of the pores and do not enter to the other one (molecular traffic control) (Figure 6b). Otherwise, the ends of the straight-chain alkanes may enter simultaneously into two (or more) adjacent pores (Pore mouth & key-lock selectivity) (Figure 6c) [49–53].

In addition to the previous two classifications, some effects related to the interactions on the outer surfaces of zeolites were studied and formulated by Chen et al. [54], including the window or cage effect (Figure 6d), to understand how the shape selectivity of erionite affects the product distribution of cracking of linear alkanes ($C_{16}H_{22}$–$C_{36}H_{74}$). This phenomenon attempts to explain the differences in diffusion rates of n-paraffin having various chain lengths inside a particular zeolite structure, which are referred to as "up and down" diffusivity variations. Generally, as the chain length of the n-paraffin increases, its diffusivity within the zeolite structure decreases due to the higher steric hindrance [55]. Derouane [56] also formulated the nest effect (Figure 7), which tried to explain the non-shape selectivity of zeolite at transition-state intermediates formation that occur within the cavities located at the ends of the pores.

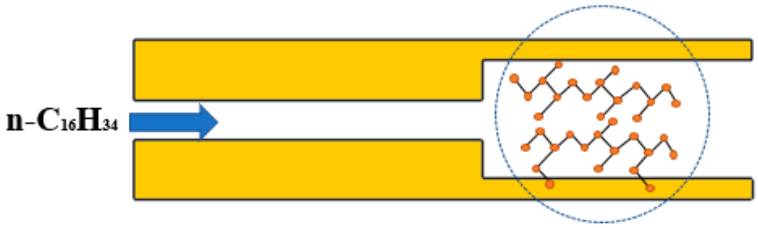

Figure 7. Representation of the nest effect in zeolite.

Various approaches have been established to manipulate the morphological characteristics of zeolites based on using and developing new structure-directing agents in order to gain a better distribution of products of n-hexadecane hydroisomerization. Several of these approaches have led to acceleration of hydrocarbons' transport within the crystals, and eventually to decreasing the residence time of intermediate alkylcarbenium in microspores and the rate of secondary cracking.

Romero D. et al. [57] observed the effect of member ring (MR) size of the zeolite framework on the selectivity of n-C_{16} hydroisomerization over 3D-10MR ZSM-5 (bulk and nanostructured), 1D-12MR ZSM-12, 1D-10MR ZSM-22 and extra-large intersecting pores (10MR + 21MR) EMM-23. Zeolite ZSM-5 having hierarchical structure and shorter intercrystalline length (higher diffusion rate) demonstrates an upgraded shape-selectivity for di-branched isomers (dimethyl) cracking owing to a snug fit of isomers at (straight-zigzag) channel intersections in the ZSM-5 framework. This shape of intersections is absent in the framework of ZSM-22; however, the cracking of di-branched isomers could be explained by the pore mouth type of shape-selectivity. The wide size of the 12MR pores provides an acceptable performance of ZSM-12, whilst in the case of EMM-23 the 10MR pores prevailed over the framework at the expense of 21MR, as a result of molecular defects of silanol groups.

Table 6 shows ZSM-12 prepared using various types of organic templates giving different morphological and acidic properties of zeolite. For instance, ZSM-12 with high specific area (>300 $m^2.g^{-1}$) and good total acidity (~200 µmol/g) with low Si/Al ratios (~40) is synthesized applying template comprising tetraethylamonium cations (like TEABr and TEAOH). In contrast, samples prepared with MTEACl and MTEABr as templates have high specific area with Si/Al ratios near to 70, to increase their acidity up to 300–700 µmol/g. As for ZSM-22, the majority of researchers use 1,6-diaminohexane as the template, giving zeolite with good crystallinity and optimal textural properties. With regard to ZSM-23, it may be produced using template comprising amide and amine functional groups, however, the last type has proven its superiority with Si/Al = 100–150 despites of the weak acidity of the zeolite produced.

Table 6. The morphological properties of zeolite-based catalysts of hydroisomerization prepared with using various organic structure-directing agents (OSDAs).

Zeolite Support Type	OSDAs	Si/Al	Specific Area [a], $m^2 \cdot g^{-1}$	Total Pore Volume [b], $cm^3 \cdot g^{-1}$	Total Acidity [c], µmol/g	Ref.
ZSM-5	Tetrapropylammonium hydroxide	32	371	0.232	238	[58]
ZSM-12	Tetraethylammonium bromide (TEABr)	45 60 90 120	310 270 220 260	N/A	195 92 80 54	[59]

Table 6. *Cont.*

Zeolite Support Type	OSDAs	Si/Al	Specific Area [a], $m^2 \cdot g^{-1}$	Total Pore Volume [b], $cm^3 \cdot g^{-1}$	Total Acidity [c], µmol/g	Ref.
ZSM-12	Methyltriethylammonium chloride (MTEACl)	25 40 50 75 100	280 293 287 314 323	N/A	720 530 430 300 270	[60]
ZSM-12		45	301	0.160	601	[61]
ZSM-12	Tetraethylammonium hydroxide (TEAOH)	40 50 71 100	323 331 300 291	N/A	N/A	[62]
ZSM-12	Benzyltrimethylammonium chlorid (BTMACl) TEABr Methyltriethylammonium bromide (MTEABr)	~90	260 220 260	N/A	107 80 115	[63]
ZSM-12	TEAOH MTEACl	61 94	258 380	0.120 0.230	N/A	[64]
ZSM-12	P-Phenylenedimethylene-bis(N-methylpyrrolidinium) dibromide P-Phenylenedimethylene-bis(N-methylpiperidinium) dibromide	20 50	297 306	0.370 0.340	898 550	[65]
ZSM-22	1,6-diaminohexane (+Organosilane) (+Silanized silica beads)	76 72 72	258 257 251	0.210 0.190 0.230	N/A	[66]
ZSM-22	1,6-diaminohexane (with acid treatment)	46	229	0.320	N/A	[67]
ZSM-22	1,6-diaminohexane	40 60 100	240 255 244	N/A	192 145 95	[68]
ZSM-22	6-amino-1-hexanol	35 50 100 150	110 137 134 144	0.210 0.190 0.140 0.120	150.2 121.7 83.2 59.1	[69]
ZSM-23	N,N-dimethylformamide	40	150	N/A	N/A	[70,71]
ZSM-23	Pyrrolidine (PY)	100 150	305 228	0.280 0.230	68 * 52 *	[72]
ZSM-23	Isopropylamine (IPA)	200	206	0.260	49 *	
ZSM-23	Dual-OSDA (PY + IPA)	100 150 200	278 282 251	0.190 0.200 0.200	22 * 19 * 17 *	
EU-1	Hexamethonium bromide	25	325	0.160	847	[61,73]
IM-5	1,5-bis(methylpyrrolidinium)-pentane bromide	33	338	0.257	289	[58]
IM-5 (micro-pores)		21	381	0.412	252	
SAPO-11	Dipropylamine phosphate ($DPA.H_3PO_4$)	0.24	209	0.134	245.3	[74]
SAPO-31	Di-n-butylamine	0.6	222	0.144	57.9	[75]
BETA	(TEAOH)	20 30 40 50	648 614 591 553	0.341 0.314 0.277 0.271	850 830 580 490	[76,77]

[a] Calculated by BET method. [b] Obtained using t-plot method at p/p_0 = 0.99. [c] Obtained using FTIR data of pyridine absorption considering bands at 1545, 1490, and 1445 cm^{-1}. * Obtained by NH_3-TPD considering peaks centered at 441–445 °C, 313–348 °C, and 220–230 °C.

The wide pores are not always preferred, where it could allow secondary reactions to happen. For instance, 12MR zeolites have the capability to accommodate mono-, di- and multi-branched hydrocarbons. However, multi-branched hydrocarbons are prone to undergoing cracking reactions [78,79].

An optimal hydroisomerization catalyst provides a high yield of isomerized products alongside the decreasing of cracking products formation (Figure 8). As a result, 10MR zeolites-based catalysts have been identified as the preferred catalyst because they allow unhindered diffusion of monobranched hydrocarbons while discouraging diffusion of multi-branched hydrocarbons via shape selection, promoting superior isomerization selectivity. Zhang M. et al. [80] studied different 10MR zeolites (ZSM-22, -23, -35 and -48)—corresponding topologies (TON, MTT, FER and MRE respectively)—as catalysts' supports n-C_{16} hydroisomerization reaction. The products distribution of n-C_{16} hydroisomerization over 10MR zeolites was significantly influenced by tiny distinctions in the channel configuration.

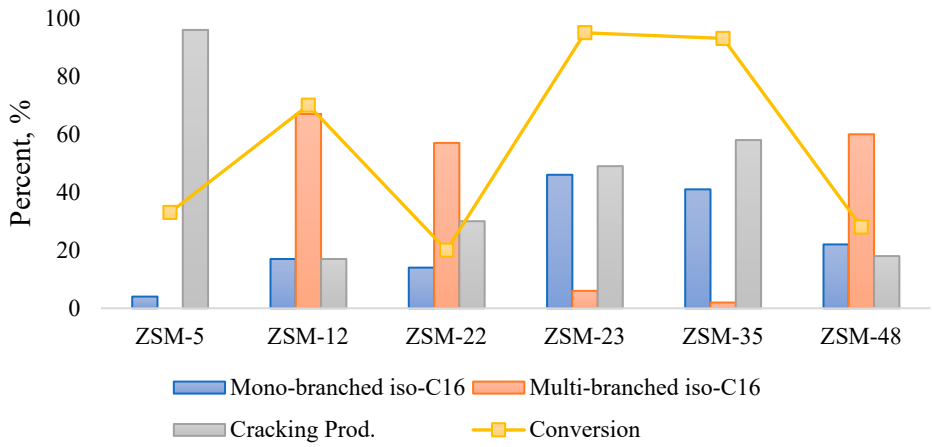

Figure 8. Product distribution of n-C_{16} hydroisomerization over 0.5% Pt/ZSM-5, -23, -35, 48 and 0.5% Pd/ZSM-12, -22 [58,79,80].

The predominated hydroisomerization product was primarily 2-methylpentadecane. This likely occurred due to fast diffusion of 2-methylpentadecane. 4-Methylpentadecane and 5-methylpentadecane were not observed in products obtained over the ZSM-22-based catalysts, due to the smallest pore size in zeolite of this type.

The hydroisomerization mechanism might be explained by the pore mouth reaction pathway due to the lack of detection of multi-branched isomers. These results are supported by the study of Zhang et al. [79], in which three different types of zeolites were tested (ZSM-12, ZSM-22 and Beta) as supports of 0.5 wt. % Pt catalysts. 1D-10MR-ZSM-23 gave the highest concentration of mono-branched C16 isomers, whereas ZSM-12 and ZSM-48 zeolites gave the highest concentrations of multi-branched isomers. These could be described by pore channel sizes for ZSM-12 and ZSM-48 (0.57 × 0.61 mm and 0.53 × 0.56 mm respectively). Significant isomerization yields have been reported with non-interconnected mesopore zeolites and zeotypes, such as ZSM-12, IZM-2 and ZSM-23 [81,82].

3.2.2. Effect of the Active Metal Site

In the literature, much attention is given to the impact of the metal precursor and its loading on the catalyst selectivity (Table 7). The metal precursor utilized in synthesis can also contribute to heterogeneities in the metal structure obtained on both bulk and nanometer scales, which are referred to as precursor effects [83–85]. Distinct characteristics of each metal precursor, such as its decomposition temperature and interaction with the support, can significantly affect the distribution of metal particles across the support and the particle size distribution [86]. As a result, the metal to acid site ratio (n_M/n_A) within

the sample varies. Ultimately, this can have a substantial impact on the performance of a catalyst [87–90]. In contrast, when considering the specific n-paraffin and operating conditions, the performance of bifunctional catalysts depends not only on the zeolite utilized but also on the ratio of metal/acid sites [25,91]

Table 7. The performance of zeolite-based catalysts of hydroisomerization prepared with using various metal precursors.

Bifunctional Catalyst	Metal Loading, %	Precursor	Si/Al	Conversion, %	Selectivity to i-C_{16}, %	Ref.
Pt/ZSM-12	0.50	$[Pt(NH_3)_4](OH)_2$	45 60 90 120	88 88 86 85	86 87 87 92	[59]
Pt/ZSM-12	0.50		90	82	87	[63]
Pt/ZSM-22	0.50	$Pt(NO_3)_2$ H_2PtCl_6 $Pt(NH_3)_4Cl_2$	100	33 32 30	52 72 45	[88]
Pt/ZSM-22 (Pt nanocrystals) Octahedral Spherical Cubes	0.50	H_2PtCl_6	100	30 35 32	71 56 53	[92]
Pt/ZSM-22	0.46	$[Pt(NH_3)_4](NO_3)_2$	N/A	60	85	[93]
Pt/BETA	0.70			26	76	
Pt/SAPO-11	0.90			90	75	
Pt/SBA-15 + BETA	0.50	H_2PtCl_6 $[Pt(NH_3)_4](NO_3)_2$ $Pt(NH_3)_4Cl_2$	SBA(7) BETA(75)	80 80 80	70 85 60	[94]
Pt/Fe/ZSM-23	0.98:0.98 1.00:1.90 0.99:3.66 1.03:7.00	H_2PtCl_6 $Fe(NO_3)\cdot 9H_2O$	50	57 70 64 62	80 82 65 64	[95]
Pt/ZSM-22/ZSM-23 (40:60)	0.50	H_2PtCl_6	100	58	78	[96]
Ni/ZSM-48	N/A	$Ni(NO_3)_2\cdot 6H_2O$	200	60	50	[97,98]
Pt/SAPO-11	0.50	H_2PtCl_6	0.24	96	58	[74]

Table 7. *Cont.*

Bifunctional Catalyst	Metal Loading, %	Precursor	Si/Al	Conversion, %	Selectivity to i-C_{16}, %	Ref.
Pd-Ni2P/SAPO-31	0.05 Pd 4.00 Ni2P	$Pd(NO_3)_2$ $(NH_4)_2HPO_4$ + $Ni(NO_3)_2$	0.6	83	72	[75]
Pt/(SAPO-11/Al_2O_3) SAPO-11:Al_2O_3 = 0.43 0.67 1.00	1.00	H_2PtCl_6	0.015 0.020 0.025	50 56 57	99 99 99	[99]

Table 7 shows that changing Si/Al—using $[Pt(NH_3)_4](OH)_2$ as a metal precursor—does not effect the performance of ZSM-12 especially on the side of conversion, but on the other

hand, the selectivity slightly improves with increasing ratio Si/Al. Also the use of different metal precursors greatly affects the selectivity of zeolite ZSM-22, as the case of using $Pt(NO_3)_2$, $Pt(NH_3)_4Cl_2$ and H_2PtCl_6, it is clear that the latter offers the best selectivity. In general, it is obvious that the best metal loading for all zeolite-based catalysts is 0.50% achieving an optimum balance between metal and acidic functions along with obtaining and guarantee the high dispersion of metal on the support.

3.2.3. Effect of the Acidity

The zeolite framework contains exchangeable cations, which play an important role on the neutralization of the charge produced by isomorphous substitution (Figure 9). For example, the substitution of Si^{+4} with Al^{+3} leads to the formation of bridging [Si-OH-Al] hydroxyls, which acts as a Brønsted acid sites (BAS) providing the catalytic activity of zeolites [100]. The removal of the 4-coordinate Al associated with the BAS via dealumination results in the formation of extra-framework Al (EFAL) species within the pores, which often function as Lewis acid sites (LAS) [101–103]. These EFAL species have been found to modify the thermal stability of zeolites and enhance their catalytic activity. Notably, the hydrothermally dealuminated Y zeolite (USY) serves as a general catalyst in the fluid catalytic cracking process.

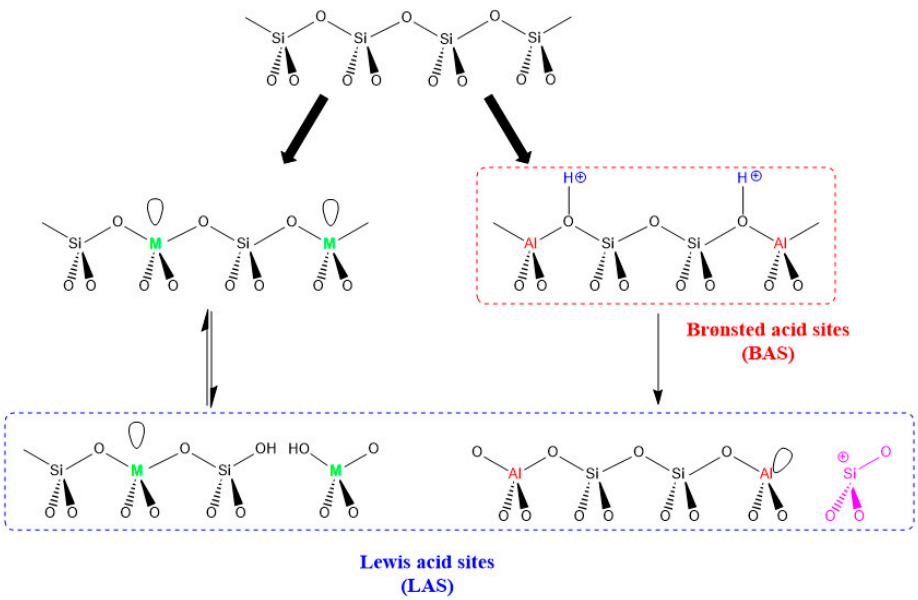

Figure 9. Developing the acid sites in the zeolite framework by cation substitutions.

Moreover, extra-framework or framework-incorporated metals, such as Ga, B, Ti, and Sn, may form LAS. These metals frequently provide zeolites with bifunctionality characterized by both redox property and acidity, which extends their application beyond petrochemistry to biomass transformation [104–106].

Achieving a balance between the density and strength of acidic sites is critical for the reactivity and selectivity of hydroisomerization reactions, and catalysts with optimal hydrogenation capacity and suitable acidity are preferred [107,108]. Aluminosilicate zeolites with medium pores have significant activity and selectivity for the isomerization of long-chain n-alkanes. However, excessive acidity may lead to cracking reactions, and extensive efforts have been made to modify the acidity via improved synthetic methods or post-treatments, such as altering acid site distribution using mixed zeolitic catalysts, among others [109].

A catalyst with high acidity could cause both hydroisomerization and hydrocracking processes, resulting in lower isoparaffin yields and the breakdown of long-chain n-paraffins to obtain less valued and lighter products. To promote hydroisomerization and suppress hydrocracking, a catalyst with the strong hydrogenation activity and moderate acidity is ideal. Furthermore, the size of the pore aperture in zeolites may have a substantial

impact on catalyst selectivity. In the case where pore sizes are small enough to prevent larger iso-paraffin formation at the acid sites, the catalyst will be good on converting n-paraffins [110].

Over the past few decades, researchers have emphasized the significant influence of the zeolite acidity of hydroisomerization catalysts on their activity and selectivity [111–113]. The general consensus is that a proper balance between hydrogenation and acid functions is essential to maximize isomer yields. However, the role of acid site density and strength remains a subject of debate due to variations in zeolite structure and reaction conditions [114]. For instance, in the case of hydrogen spillover highlights, the olefinic intermediates formed on acidic sites can be hydrogenated with H adsorbed over the far Pt cluster, and as a result, the physical mixture of Pt/SiO_2 and zeolite can exhibit good selectivity. Batalha et al. [115] propose that catalyst selectivity is determined by the intimacy between metal and protonic sites, which is the number of acid sites that olefinic intermediates encounter during diffusion between two metallic sites.

The acidity of zeolites can be adjusted by altering the ratio of SiO_2/Al_2O_3. Furthermore, some alkaline earth metals (Ba [116], Mg [117]) and transition metals (Fe [118]) can be included into the structure to decrease the acidity; the same effect exerts coating the zeolite with alumina [119].

4. Impact of Operating Parameters on Process Efficiency

The operational conditions of hydroisomerization of the diesel fraction are largely influenced by the composition of feedstocks and the desired quality of the final product. However, the choice of catalyst is equally critical. Initially, the hydroisomerization process was performed at high hydrogen pressures ranging from 10 to 25 MPa. Upon the development of more active catalysts, however, the pressure requirements have been reduced to 4–5 MPa.

The temperature of the process is determined by both the boiling range of the feedstock and the activity of the catalyst. Usually, higher boiling fractions necessitate higher process temperatures. The application of highly efficient zeolite-based catalysts has enabled a significant temperature reduction in recent years. For example, kerosene fractions are processed at temperatures ranging from 240 to 280 °C, as opposed to previous temperatures as high as 450 °C. Thus, the progress of the hydroisomerization process could be defined as a trend to significant reduction of temperature and pressure due to the use of more active catalysts. Despite numerous investigations in the field of knowledge, there is a relatively limited understanding of the interconnected influence of these operational parameters. Usually, experiments are performed by varying temperature within a predetermined range while keeping the remaining parameters fixed. Consequently, the predominant impact of temperature variation on catalyst performance can be observed. In general, with rise in temperature, conversion increases, but selectivity decreases (Figure 10).

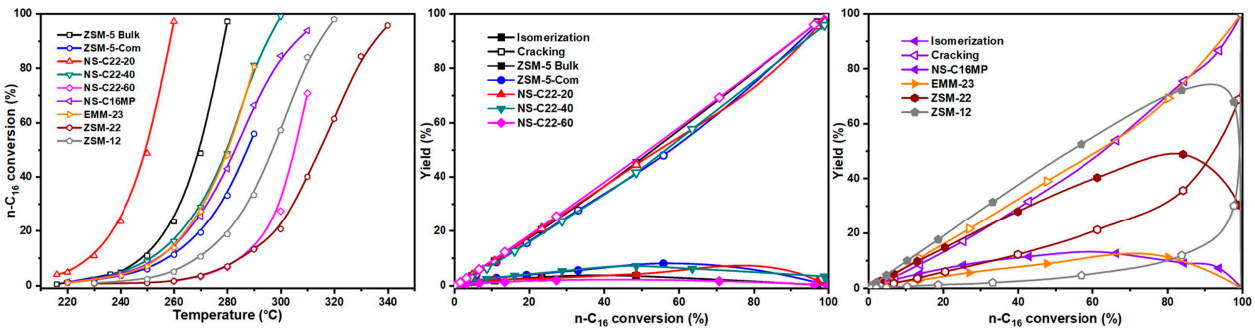

Figure 10. Performance of zeolite-based catalysts (~1 wt% Pd) for hydroisomerization of n-C_{16} at the operating condtions: temperature 220–340 °C, WHSV = 10 h^{-1}, H_2/n-C_{16} = 20, P = 6 MPa. Reprinted with permission from [57]. Copyright 2020 Elsevier Inc.

Typically, recent studies of n-hexadecane hydroisomerization have performed at temperature range of 200–380 °C, operating pressure up to 6 MPa, the weight hourly space velocity (WHSV) between 1–6 h^{-1}, and H_2/n-C_{16} ratios ranging from ~10 up to 1000.

As Table 8 shows, the majority of catalysts operate at temperature of at least 270 °C and pressure exceeding 2 MPa. Analysis of the performance of catalysts above reveals that zeolites ZSM-12, ZSM-22, and SAPO-11 at temperatures above 310 °C and ZSM-23 at temperatures between 270 and 290 °C are superior supports for platinum-impregnated catalysts. In contrast, zeolites SAPO-11, SAPO-31, and SAPO-41 at temperatures exceeding 340 °C are preferable for palladium-impregnated catalysts, while catalysts supported with BETA, USY, and mordenite have the modest performance.

However, ZSM-5 supports demonstrated the worst selectivity (whatever type of active metal) even in the nanostructural form. As for the effect of pressure change, it depends on the type of zeolites. For example, in the case of ZSM-5, the increase in pressure from 2 to 6 MPa has affected remarkable effect on the conversion of n-alkanes. On the other hand, in the case of ZSM-22, the effect of pressure is somewhat proportionally limited on the reaction conversion and selectivity. However, the effect of WHSV and H_2/n-C_{16} is still unclear considering that they have not ever been the main objectives of any investigation.

Parmar et al. [116] studied the impact of increasing WSHV on the performance of bifunctional catalysts comprising Pt/ZSM-22 modified with Group-II cations (Ca^{+2}, Ba^{+2}, Mg^{+2}). Their findings revealed that higher WSHV and temperatures > 300 °C led to a decrease in the conversion and an increase in selectivity towards iso-paraffins C_{16}. This observation can be due to the shortened reaction time, which has a negative impact on both the main (isomerization) and secondary (cracking) reactions. Subsequently, Zhang et al. [80] investigated the impact of WHSV at temperatures below 300 °C on the performance of different Pt-impregnated 10MR zeolites. These data confirmed an advantageous effect of increasing WHSV for both MTT and FER zeolite types (Pt loadings ~0.93 wt %), resulting in improved selectivity. This phenomenon can be attributed to the suppression of cracking iso-paraffins C_{16}. In contrast, increasing WSHV led to a decrease in selectivity for both TON and MRE zeolite types (Pt loading ~0.91 wt %), due to the lesser content of Brønsted acid sites.

Table 8. The performance of zeolite-based catalysts of hydroisomerization at optimal operating conditions.

Bifunctional Catalyst	Active Metal Loading, %	Si/Al	Optimal Conditions				Conversion, %	Selectivity, %	Ref.
			T, °C	P, MPa	WHSV, h^{-1}	H_2/n-C_{16}			
Pd/ZSM-5	1.00	40	280	6.0	10.0	20	95	4	[57]
Pd/ZSM-5 [a]	1.00	61	290				58	16	
Pt/ZSM-5	0.50	32	240	2.0	6.0	10	33	4	[58]
Pt/ZSM-12	0.50	90	310	6.0	1.1	10	86	87	[63]
Pd/ZSM-12	1.00	62	310	6.0	10.0	20	85	92	[57]
Pt/ZSM-22	0.46	N/A	320	4.0	N/A	N/A	80	85	[93]
Pd/ZSM-22	1.00	61	330	6.0	10.0	20	85	56	[57]
Pt/ZSM-22	0.45	45	305	6.0	0.7	10	94	76	[120]
Pt/Ca-ZSM-22	0.42		312				91	82	
Pt/Ba-ZSM-22	0.44		312		1.1		90	86	
Pt/ZSM-22	0.90	100	300	4.0	N/A	600	15	33	[81]
Pt/ZSM-23	0.91		290				70	80	
Pt/ZSM-23	0.60	60	270	3.0	1.0	6	91	82	[117]
Pt/ZSM-23	0.50	58	290	3.0	2.0	1000	85	85	[121]
Pd/EMM-23	1.00	60	290	6.0	10	20	80	13	[57]
Pt/ZSM-35	0.95	40	300	4.0	N/A	600	92	48	[80]
Pt/ZSM-48	0.93	200					20	54	

Table 8. *Cont.*

Bifunctional Catalyst	Active Metal Loading, %	Si/Al	Optimal Conditions				Conversion, %	Selectivity, %	Ref.
			T, °C	P, MPa	WHSV, h^{-1}	H_2/n-C_{16}			
Pt/EU-1/ZSM-48	0.97	200	300	4.0	N/A	600	80	55	[122]
Pt/SAPO-11 [b]	0.15	0.6	310	2.0	3.1	650	94	96	[123]
Pt/SAPO-11	0.90	N/A	350	4.0	N/A	N/A	90	75	[93]
Pd/SAPO-31	0.15	0.3	340	2.0	3.7	500	90	90	[124]
Pd/SAPO-41	0.80					8	90	96	[125]
Pt-Pd/SAPO-41	0.15:0.35						96	94	[126]
Pd/SAPO-41	0.10	0.3	360	2.0	3.7	500	87	95	[127]
Pd-Ni_2P/SAPO-31	0.05/4.00	0.3	380	2.0	3.7	500	85	87	[75]
Pt/IM-5	0.50	33	240	2.0	6.0	10	43	5	[58]
Pt/BETA	0.40	14	200	0.5	3.0	13	50	63	[128]
Pt/BETA	0.79	-	280	4.0	N/A	N/A	50	70	[93]
Pt-Pd/BETA	0.40/0.40	25	200	0.1	3.0	750	78	93	[129]
CoMo/Al_2O_3-Y	3.50–13.00	2.5	360	1.5	1.0	150	11	55	[130]
Pt/BETA	1.00	14	200	0.5	3.0	13	50	68	[117]
Pt/USY	0.70	17	215					61	
Pt/USY+ Pt/BETA	0.70/1.00	14/17	205					65	
Pt/Al-SBA-15 + BETA	0.50	75	300	5.0	3.5	5	84	71	[131]
Pt/Al-SBA-15 + MOR		45					43	81	

[a] Nanostructure. [b] Vacuum-assisted synthesis.

Upon the investigation of n-hexadecane hydroisomerization over Pd-Pt/β-zeolite catalyst, Bauer et al. [129] observed a decline in the conversion from 89.0% under pressure of 3 MPa to 53.0% at 7.5 MPa. This result can be attributed to the competition of olefinic intermediates with hydrogen adsorbed over active sites under high-pressure conditions. Although higher hydrogen pressures have a negative impact on the conversion of n-paraffins and provide minimal enhancements in selectivity and catalyst stability, it should be noted that industrial specifications are usually required to exploit catalysts within the pressure range of 3–5 MPa.

5. Tolerance of Bifunctional Catalysts to Poisons and Deactivation

5.1. The Effect of Impurities-Containing Feed

Commercial feedstock is frequently impaired with nitrogen- and sulfur-containing compounds, which could damage the metallic and acidic active sites of bifunctional catalyst [132]. Nitrogen poisoning is a serious issue in catalysis, especially with zeolite-based catalysts employed in n-hexadecane isomerization. Understanding the forms of nitrogen adsorption and the further blocking of active sites allows us to understand the mechanisms that govern catalyst deactivation and selectivity loss. The deactivation of bifunctional catalysts on hydroisomerization of n-hexadecane with sulfur and nitrogen compounds has got some attention, but the understanding of their impacts on catalytic isodewaxing is unclear [133,134].

According to Lee et al. [135] the polymetallic bifunctional Pt-Pd-Mg/ZSM-23 catalyst exhibited a high stability of product properties for more than 30 days in the presence of sulfur impurities (1–2 wt.%).

Pimerzin et al. [136] examined the stability of two type of SAPO-11-supported bifunctional catalysts (transition metal sulfides and noble metal) for the isomerization of hexadecane. Nitrogen-containing feedstock inhibits isomerization catalytic activity more strongly, and whether the quantity of sulfur in the feedstock is equivalent to or higher than 100 ppm, transition metal-based bifunctional catalysts surpass Pt-catalyst in n-hexadecane isomerization (Figure 11).

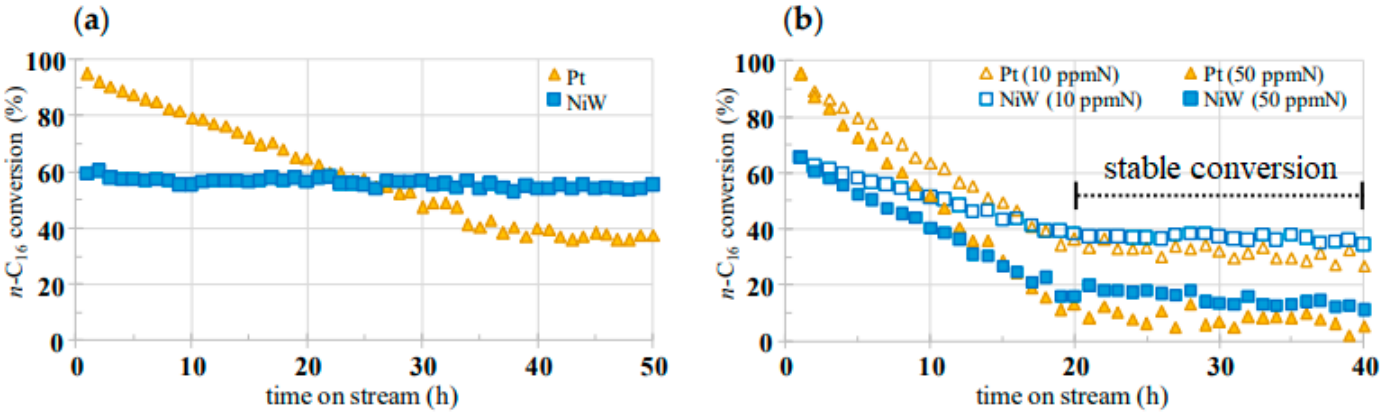

Figure 11. The stability of the conversion of bifunctional catalysts on processing feedstocks containing sulfur (**a**) and nitrogen (**b**). Adapted with permission from [136]. Copyright 2020 MDPI.

Later, the effect of nitrogen-containing feed was retraced by Vinogradov et al. [130] with different zeolite-supported catalysts (ZSM-5, Beta, and Y). It was observed that the nitrogen impurities (quinoline) could play a role as a selective-controlling agent, as a result of the predominant adsorption of quinoline on strong acid sites performing the cracking process.

5.2. The Impact of Water

The effect of water-containing feed on the process of hydroisomerization of n-alkanes was considered recently [137–139]. Controlled amounts of water and iso-pentanol promoted the performance of FAU-type structured zeolite (with rare-earth metal—REM) in the hydroconversion of n-hexadecane [140]. According to the results, the support was activated by creating new protonic active centers via the hydration of REM cations. However, due to competing adsorption and hydrating protons located in the zeolite, water decreases acidic strength and deactivates the catalyst.

The impact of competing water adsorption on the acid sites of Pt/MFI, Pd/MFI, and Pt/HY was investigated by Brosius et al. [141]. Authors discovered that water prevented n-hexadecane cracking products from the secondary isomerization. Moreover, in the case of using Pt(0.9 wt%)/HY products with a great extent of branching were obtained. In contrast, Pt(0.9 wt%)/MFI produced a wider extent of linear products (Figure 12).

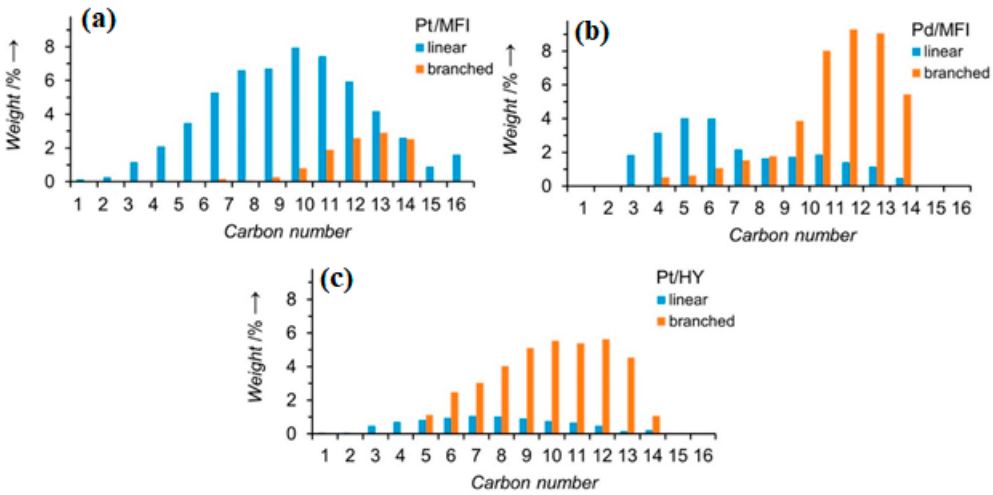

Figure 12. Distributions of n-hexadecane hydrocracking products (cracking yield 55%) with water over (**a**) 0.9% Pt/MFI and (**b**) 0.9% Pd/MFI and (**c**) (cracking yield 44%) over 0.9% Pt/H-Y. Reprinted with permission from [141]. Copyright 2016 American Chemical Society.

5.3. Deactivation by Coke Deposition

Upon the hydroisomerization of n-alkanes over zeolite-based catalysts, carbonaceous deposits are obtained as a result of complicated chain of reactions, namely the oligomerization, cyclization, and condensation of alkylaromatics to generate polycyclic aromatics (Figure 13) [142–145]. Coke is composed of heavy components that are extremely deposited as a byproduct on the surface of the zeolite, poisoning the active sites and clogging the pores. It was observed that the interaction between intermediates of coking and other reactions intermediates impacts on the distribution and selectivity of the products. Coking occurs faster on strong acid sites than on weak acid sites, because the last are less sensitive to coke formation [146,147].

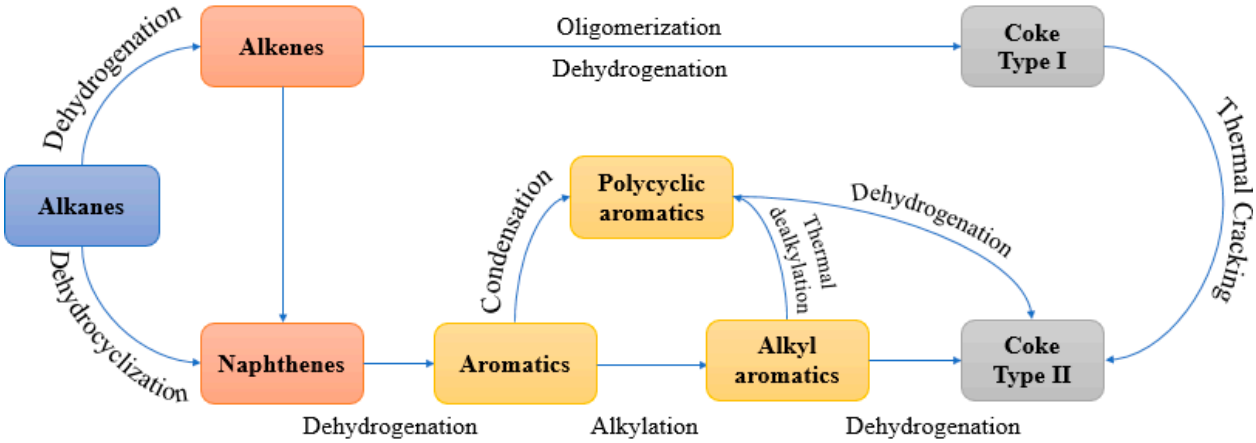

Figure 13. General illustration of the routes of the coke formation over bifunctional catalysts.

The coke can be formed in one of three ways: (a) synchronously with the desired reaction (competitive phase), (b) consecutively to the directed reaction (successive phase), or (c) both of (a + b) simultaneously [145]. Coke combustion can renew the catalyst, however, the intense regeneration conditions and the presence of water prevent full catalytic activity from being regained [148].

Bauer and Karge [149] proposed a classification system that differentiates between two forms of coke obtained. Condensation, oligomerization, and alkylation processes involving reactants and their intermediates produce "Coke-type I" at lower temperatures. "Coke-type II" is found at higher temperatures and comprises chemical stages requiring greater activation energies, such as dehydrocyclization, thermal cracking, and dehydrogenation.

The coke formation rate is influenced by the same parameters as the rate of the catalytic reaction itself. These parameters encompass the nature of the reactants [150,151], the pore structure of the catalyst [152], the density of the active sites [151,153], and the operating conditions [153].

Carbonaceous deposits are thought to disable the catalyst by poisoning the active sites or by pore blockage [154], but the latter causes more severe deactivation than active site poisoning [155], because one active site per coke molecule can be deactivated, but pore clogging with a single carbonaceous molecule could limit or prohibit reactant molecules from accessing all active sites inside the clogged pore.

The coke may accumulate via three ways: (a) uniform surface deposition [156], (b) pore-mouth blockage [157], and (c) bulk-phase blockage [156,158]. Each mode has a particular effect on the diffusivity of reactants and, as a result, on catalytic activity.

In the case of uniform surface deposition, it has been hypothesized that carbonaceous deposits are uniformly distributed throughout the micropore channels of catalyst. Nonetheless, this distribution is likely to shorten the micropore diameter decreasing the diffusion rate and catalytic activity. According to the pore-mouth blockage scenario, carbonaceous deposits tend to build at the pore entrances, limiting access for the reactant to the active sites within the pore. Although the pores are not totally blocked, this process reduces the

diffusion rate. In this situation, carbonaceous deposits cover a tiny fraction of active sites, in which productivity will be proportional to the number of accessible active sites [157]. The bulk-phase blocking scenario incorporates both of the aforementioned carbonaceous deposition mechanisms. However, in this instance, a large quantity of coke is generated on the outer surface of catalyst, resulting in full clogging of the pores.

During the catalytic cracking of n-hexane and 1-hexene over ultrastable Y zeolite, Chen and Manos [159,160] differentiated coke into coke precursors and hard coke. Coke precursors are easily volatilized in inert nitrogen and removed off the catalyst sample, whereas hard coke stays on the catalyst even at high temperatures (600 °C) and is removed by burning. Bauer et al. [129] investigated the formation of coke depositions during the hydroisomerization of n-hexadecane on the Pt-Pd/H-beta bifunctional catalyst. It was revealed that both the volume and surface area of micropores were decreased by roughly 8% after 62 days on-stream as a result of pore occlusion with coke.

Bifunctional catalysts including mesopores have enhanced the lifetime. In the most cases, deactivation is caused by pore-mouth occlusion by carbonaceous deposition. Numerous studies have claimed that the favorable effect on the lifetime is due to an increased tolerance to the impacts of coke rather than a lower rate of the coke formation. Shortening diffusion lengths combined with increased pore openings in the mesoporous makes the pores more resistant to blocking, which may explain the reduced effects on coking. This simple reasoning, however, may not fully describe the situation. Holm et al. [161] reasoned that, due to mesoporosity, products obtained will have a shorter retention time in the micropores, potentially suppressing subsequent secondary coking.

6. Cost-Effective and Eco-Friendly Synthesis Approaches

Conventional methodologies for zeolites synthesis have been extensively documented in the scientific literature [162]. However, numerous challenges exist, including the high expenses associated with structure-directing agents and starting materials, energy consumption and, recycling wastes. Moreover, the multistage production comprising expensive procedures hinders commercialization [163–165]. As a result, the synthesis of hierarchical zeolites using an environmentally friendly approach has gained attention [166,167]. Reliable syntheses aim to accommodate the effectiveness of conventional methods with strategies that reduce environmental impact, such as utilizing alternative starting materials, carrying out solvent-free or template-free syntheses, and reusing water [168–170].

Recent studies have reported the successful synthesis of hierarchical zeolites using an eco-friendly approach [171,172]. These works have demonstrated the feasibility of zeolite production through the application of green chemistry principles. However, certain drawbacks have also been observed, including low crystallinity, non-uniform pore structures, and reduced process efficiency (Table 9).

Significant efforts have been devoted to establishing the connections between the characteristics and catalytic performance of zeolites, driven by their economic significance. In this regard, the development of innovative syntheses and alternative raw materials have a focal point. An example of a recent eco-friendly approach is template-free synthesis, which has been tested for the production of the MFI framework structure [173–175]. Notably, tubular clay nanomaterials, specifically Halloysite, have been utilized as triple-functional materials: the source of alumina and silica, and hard template [176–180]. It should be noted that bioresources, such as water reeds (Phragmites) [181] and rice husk ash [182–187], mineral sources including rectorite [188] and diatomite [189,190], and industrial wastes like coal fly ash [191,192], have a minor scale, but employed as sources of silica and alumina in the synthesis above. This advancement represents a notable step forward in green chemistry for zeolite production.

Table 9. Comparison of traditional and modern approaches of zeolite-based catalyst production.

Approach	Principle	Influencing Factors	Advantages	Disadvantages
Solvothermal method	Using solvents	Temperature, pressure, reactants sources and compositions, Si/Al, aging time, alkalinity, stirring conditions, seeding, solvents type	Simple; cheaper	Environmentally harmful; energetic and time-consuming approach
Alkali-fusion method	Fussing raw materials with alkali before hydrothermal treatment	Si/Al, concentration of the alkali medium, temperature of crystallization	Using low-grade raw materials without purification; offers the zeolite with high purity	High energy consumption; expensive; multistep; time-consuming
Sol-gel method	Formation of an inorganic sol and its gelation in liquid phase gel to form a 3D structure	Hydrolysis rate, temperature, heating rate, PH	High-quality product; homogeneity; does not require expensive equipment	Cost of precursors
Microwave method	Using microwave irradiation	Si/Al ratios, alkalinity, wavelength, temperature, crystallization time	Concise time; high purity product; small particle size	Low crystal aspect ratio
Ultra-sound method	Using ultrasound with frequency 20 kHz–2 MHz	Duration and frequency of ultrasonication	Very simple; rapid reaction; high crystals growth rate; suitable particle size distribution and morphology; control on nucleation process	The mechanism of ultrasonic effect remains unclear

Occasionally, traditional synthesis approaches necessitate substantial quantities of organic or water-based solvents that are economic and ecological drawbacks, particularly evident in the context of silicoaluminophosphate (SAPO) materials [193,194].

Recently, Xiao et al. effectively synthesized a variety of zeolites without the need for extra solvents. The zeolites obtained comprised SAPO-11, SAPO-20, SAPO-34), aluminophosphates (AlPO-11), metal-containing aluminophosphate zeolites (Mg-AlPO-11, Co-AlPO-11, Mg-SAPO-46, and Co-SAPO-46) [195], as well as aluminosilicates (ZSM-5, silicate-1, ZSM-49, SOD, MOR, Beta, and FAU) [196]. This innovation in synthesis indicates that it has the potential to produce a wide range of zeolite frameworks without the need for extra solvents.

Most current studies have focused on the seed-assisted approach to crystal pattern modification as a simple and ecologically benign method [197–199]. This method includes the inducing and orientation of crystals growth by adding into the gel a minor amount of the same targeted zeolite structure as a seed. This method has been shown to be successful in syntheses of zeolite frameworks such as MFI [200–203], MTW [64,204], MEL [205], FAU [206], MOR [207], CHA [208], and MRE [209].

Nonetheless, despite its potential benefits, the seed-assisted approach has several limits, such as the broad particle size distribution, tendency to particle aggregation, and possibility of pore blockage [210,211]. To maximize the efficiency and performance of the seed-assisted synthesis technique, these constraints must be handled and minimized.

Unconventional methodologies for zeolite synthesis and the ability to modify surface properties through post-treatments are two effective strategies employed to improve the zeolite performance. One such approach is microwave-assisted hydrothermal synthesis (MAHyS), which significantly accelerates synthesis. For instance, Muraza et al. [212] successfully increased the rate of synthesis of the TON framework zeolite from 66–72 hours to 24 hours using the MAHyS technique.

Another promising technique is the ultrasound-assisted synthesis of zeolites, which offers several advantages, including increased surface area and shorter synthesis time [213,214]. These effects have been confirmed in the syntheses of MCM-22 [215], ZSM-5 [182,216], and SAPO-11 [217] zeolites, where the ultrasound-assisted method promotes the dissolution of reactants and accelerates the progression of crystallization.

7. Conclusions

The isomerization of n-hexadecane and its multiple isomers is critical to upgrading the low-temperature characteristics of diesel, such as cloud point, pour point and cold filter plugging point, also enhancing the cetane number, therefore, the effective catalysts and the optimal operating conditions have been reviewed.

The concept of main and secondary types of shape selectivity was analyzed in detail. On this basis the requirements for the preparation procedure of zeolites were formulated: mainly, mesopores should possess the product shape, transition-state, and pore mouth selectivity, but pores with the reactant shape, mutual intersections, and nest effect selectivity should be excluded.

The fundamentals of mechanism of n-hexadecane hydroisomerization, characterizing zeolite were highlighted. To improve the yield, the choice of structural and morphological characteristics of catalyst, combined with the optimal balance between metal and acidic sites (n_M/n_A) have the greatest impact on the process. Large external surface area and mesoporous structures minimize the diffusion limitations and unfavorable cracking. Diffusion on a high surface area enhances adsorption at pore-mouths and improves accessibility to acid sites, resulting in better conversion and selectivity.

The effects of nitrogen-, sulfur- and water-containing feedstock on the catalyst performance were also discussed. It was concluded that sulfur plays a lesser deactivation role than nitrogen impurities as a selectivity-control agent, poisoning the acid sites and deactivating the isomerization function. In contrast, water prevents the deactivation of catalysts and suppresses cracking reactions.

The recent trend in the synthesis zeolite-supported catalysts from natural sources—such as clay and natural minerals is considered very attractive from both economic and environmental standpoints. Although it is still limited to the ZSM-5 zeolite, it promises a lot of progress in developing new types of zeolites. The novel methods for synthesis of bifunctional catalysts, and their success were discussed in overcoming the problems that may face traditional methods, despite the presence of some challenges that still exist in environmental and economic areas, and the textural and structural properties of zeolites.

Furthermore, the use of alternative feedstocks, such as renewable sources, as well as the integration of hydroisomerization to other refining processes, such as hydrotreating and hydrocracking, could open up new avenues for producing high-quality diesel fuels.

The authors thank GZ (FSZE-2022-0002).

Author Contributions: Conceptualization, Y.A., V.S. and A.G.; writing—original draft preparation, Y.A. and M.R.; writing—review and editing, Y.A., V.S. and A.G.; supervision, A.G. All authors have read and agreed to the published version of the manuscript.

Funding: This research received no external funding.

Data Availability Statement: Not applicable.

Conflicts of Interest: The authors declare no conflict of interest.

References

1. Kazakov, M.O.; Smirnova, M.Y.; Dubinin, M.E.; Bogomolova, T.S.; Dik, P.P.; Golubev, I.S.; Revyakin, M.E.; Klimov, O.V.; Noskov, A.S. Combining USY and ZSM-23 in Pt/zeolite hydrocracking catalyst to produce diesel and lube base oil with improved cold flow properties. *Fuel* **2023**, *344*, 128085. [CrossRef]
2. Viswanadham, N.; Saxena, S.K.; Panwar, R.; Ray, A. A single-step catalytic process for the production of high-octane molecules from normal paraffins using zeolite supported bi-functional catalysts. *Chem. Eng. Process. Process Intensif.* **2022**, *177*, 108990. [CrossRef]
3. Liu, S.; Zhang, L.; Zhang, L.; Zhang, H.; Ren, J. Function of well-established mesoporous layers of recrystallized ZSM-22 zeolites in the catalytic performance of *n*-alkane isomerization. *New J. Chem.* **2020**, *44*, 4744–4754. [CrossRef]
4. Li, K.; Cui, T.; Zhao, J.; Liang, C.; Li, C. Regulate the mesopores and acidic structure of Pt/USY zeolite catalyst for improved performance in the hydroisomerization of Phenanthrene to Alkyl-adamantane. *Chem. Eng. Sci.* **2023**, *279*, 118957. [CrossRef]
5. Chang, T.; Liu, S. Role of the mesoporous diameters of hierarchical ZSM-22/MCM-41 zeolite for *n*-alkane isomerization. *Mol. Catal.* **2021**, *503*, 111420. [CrossRef]

6. Li, L.; Shen, K.; Huang, X.; Lin, Y.; Liu, Y. SAPO-11 with preferential growth along the a-direction as an improved active catalyst in long-alkane isomerization reaction. *Microporous Mesoporous Mater.* **2021**, *313*, 110827. [CrossRef]
7. Mäki-Arvela, P.; Azkaar, M.; Vajglová, Z.; Aho, A.; Hemming, J.; Peurla, M.; Eränen, K.; Kumar, N.; Murzin, D.Y. Hexadecane hydrocracking for production of jet fuels from renewable diesel over proton and metal modified H-Beta zeolites. *Mol. Catal.* **2019**, *476*, 110515.
8. Mäki-Arvela, P.; Kaka khel, T.A.; Azkaar, M.; Engblom, S.; Murzin, D.Y. Catalytic hydroisomerization of long-chain hydrocarbons for the production of fuels. *Catalysts* **2018**, *8*, 534. [CrossRef]
9. Patrylak, L.; Krylova, M.; Pertko, O.; Voloshyna, Y.; Yakovenko, A. *n*-Hexane isomerization over nickel-containing mordenite zeolite. *Chem. Chem. Technol.* **2020**, *14*, 234–238. [CrossRef]
10. Akhmedov, V.M.; Al-Khowaiter, S.H. Recent advances and future aspects in the selective isomerization of high *n*-Alkanes. *Catal. Rev.* **2007**, *49*, 33–139. [CrossRef]
11. Misra, P.; Alvarez-Majmutov, A.; Chen, J. Isomerization catalysts and technologies for biorefining: Opportunities for producing sustainable aviation fuels. *Fuel* **2023**, *351*, 128994. [CrossRef]
12. Echevskii, G.; Weixin, Q.; Kodenev, E.; Toktarev, A.; Chunmei, D. Study of Bifunctional Hydrocracking and Hydroisodeparaffinization Catalysts Based on Zeolites and Alumophosphates, Part 2: Effect of the Activity of Hydrogenating and Acidic Components on the Activity and Selectivity of Hydroisodeparaffinization Catalysts. *Catal. Ind.* **2020**, *12*, 81–87. [CrossRef]
13. Liu, P.; Qiu, Z.; Shi, H.; Song, Y.; Zhao, D.; Wang, P.; Wang, T.; Bao, X. Reducing the diffusion barriers of Pt/Beta catalyzed n-hexane isomerization by SBA-15 addition and high-energy milling. *Microporous Mesoporous Mater.* **2023**, *356*, 112591. [CrossRef]
14. Worldwide Fuel Charter. *Gasoline and Diesel Fuel*; Worldwide Fuel Charter: Brussels, Belgium, 2019.
15. Do, P.T.; Crossley, S.; Santikunaporn, M.; Resasco, D.E. Catalytic strategies for improving specific fuel properties. *Catalysis* **2007**, *20*, 33–64. [CrossRef]
16. Yanowitz, J.; Ratcliff, M.A.; McCormick, R.L.; Taylor, J.D.; Murphy, M.J. *Compendium of Experimental Cetane Numbers*; National Renewable Energy Lab. (NREL): Golden, CO, USA, 2017.
17. Ribeiro, F.; Marcilly, C.; Guisnet, M. Hydroisomerization of n-hexane on platinum zeolites: I. Kinetic study of the reaction on platinum/Y-zeolite catalysts: Influence of the platinum content. *J. Catal.* **1982**, *78*, 267–274. [CrossRef]
18. Chica, A.; Corma, A. Hydroisomerization of pentane, hexane, and heptane for improving the octane number of gasoline. *J. Catal.* **1999**, *187*, 167–176. [CrossRef]
19. Kosareva, O.A.; Gerasimov, D.N.; Maslov, I.A.; Pigoleva, I.V.; Zaglyadova, S.V.; Fadeev, V.V. Effect of the Zeolite Type on Catalytic Performance in Dewaxing of the Diesel Fraction under Sour Conditions. *Energy Fuel* **2021**, *35*, 16020–16034. [CrossRef]
20. Hiraoka, K.; Kebarle, P. Stabilities and energetics of pentacoordinated carbonium ions. The isomeric protonated ethane ions and some higher analogs: Protonated propane and protonated butane. *J. Am. Chem. Soc.* **1976**, *98*, 6119–6125. [CrossRef]
21. Liu, S.; Luo, C.; Deng, X.; Fang, Y. Toward rational design of narrowly-distributed mesopore on ZSM-22 zeolite for enhanced Pt dispersion and *n*-alkane isomerization performance. *Fuel* **2022**, *328*, 125282. [CrossRef]
22. Jacobs, P.A.; Martens, J.A. Introduction to acid catalysis with zeolites in hydrocarbon reactions. In *Studies in Surface Science and Catalysis*; Elsevier: Amsterdam, The Netherlands, 1991; Volume 58, pp. 445–496.
23. Weitkamp, J. Catalytic hydrocracking—Mechanisms and versatility of the process. *ChemCatChem* **2012**, *4*, 292–306. [CrossRef]
24. Weisz, P.; Swegler, E. Stepwise reaction on separate catalytic centers: Isomerization of saturated hydrocarbons. *Science* **1957**, *126*, 31–32. [CrossRef] [PubMed]
25. Alvarez, F.; Ribeiro, F.; Perot, G.; Thomazeau, Y.C.; Guisnet, M. Hydroisomerization and hydrocracking of alkanes: 7. influence of the balance between acid and hydrogenating functions on the transformation of *n*-decane on pthy catalysts. *J. Catal.* **1996**, *162*, 179–189. [CrossRef]
26. Ravishankar, R.; Sivasanker, S. Hydroisomerization of n-hexane over Pt—H-MCM-22. *Appl. Catal. A Gen.* **1996**, *142*, 47–59. [CrossRef]
27. Kazansky, V.; Frash, M.; Van Santen, R. Quantumchemical study of the isobutane cracking on zeolites. *Appl. Catal. A Gen.* **1996**, *146*, 225–247. [CrossRef]
28. Martens, G.; Marin, G. Kinetics for hydrocracking based on structural classes: Model development and application. *AICHE J.* **2001**, *47*, 1607–1622. [CrossRef]
29. Zschiesche, C.; Himsl, D.; Rakoczy, R.; Reitzmann, A.; Freiding, J.; Wilde, N.; Gläser, R. Hydroisomerization of Long-Chain n-Alkanes over Bifunctional Zeolites with 10-Membered-and 12-Membered-Ring Pores. *Chem. Eng. Technol.* **2018**, *41*, 199–204. [CrossRef]
30. Kotrel, S.; Knözinger, H.; Gates, B. The Haag–Dessau mechanism of protolytic cracking of alkanes. *Microporous Mesoporous Mater.* **2000**, *35*, 11–20. [CrossRef]
31. Shakor, Z.M.; Ramos, M.J.; AbdulRazak, A.A. A detailed reaction kinetic model of light naphtha isomerization on Pt/zeolite catalyst. *J. King Saud Univ. Eng. Sci.* **2022**, *34*, 303–308. [CrossRef]
32. Noh, G.; Shi, Z.; Zones, S.I.; Iglesia, E. Isomerization and β-scission reactions of alkanes on bifunctional metal-acid catalysts: Consequences of confinement and diffusional constraints on reactivity and selectivity. *J. Catal.* **2018**, *368*, 389–410. [CrossRef]
33. Qi, Y.; Cai, C.-F.; Sun, P.; Wang, D.-W.; Zhu, H.-J. Crude oil cracking in deep reservoirs: A review of the controlling factors and estimation methods. *Pet. Sci.* **2023**, *20*, 1978–1997. [CrossRef]

34. Hu, W.; Noh, G.; Iglesia, E. Consequences of metal-acid site proximity for alkane isomerization and β-scission mediated by bifunctional catalytic cascades. *J. Catal.* **2023**, *425*, 125–142. [CrossRef]
35. Wu, X.; Lei, X.; Wang, S.; Zhang, H.; Cui, Q.; Bao, X.; Wang, T.; Yuan, P. Tuning the acidity and pore structures of NiP based bifunctional catalyst for efficient *n*-hexane isomerization. *Fuel* **2022**, *324*, 124396. [CrossRef]
36. Voloshyna, Y.; Pertko, O.; Patrylak, L.; Yakovenko, A. Peculiarities of palladium-containing MFI-type zeolites as catalysts of isomerization of linear alkanes. *Vopr. Khimii I Khimicheskoi Tekhnol.* **2020**, *6*, 26–32. [CrossRef]
37. Leprince, P. *Petroleum Refining. Vol. 3 Conversion Processes*; Editions Technip: Paris, France, 2001; Volume 3.
38. McKetta, J.J., Jr. *Encyclopedia of Chemical Processing and Design*; CRC Press: Boca Raton, FL, USA, 1997.
39. Del Campo, P.; Martínez, C.; Corma, A. Activation and conversion of alkanes in the confined space of zeolite-type materials. *Chem. Soc. Rev.* **2021**, *50*, 8511–8595. [CrossRef] [PubMed]
40. Gomes, L.C.; de Oliveira Rosas, D.; Chistone, R.C.; Zotin, F.M.Z.; de Araujo, L.R.R.; Zotin, J.L. Hydroisomerization of n-hexadecane using Pt/alumina-Beta zeolite catalysts for producing renewable diesel with low pour point. *Fuel* **2017**, *209*, 521–528. [CrossRef]
41. Dhar, A.; Vekariya, R.L.; Bhadja, P. *n*-Alkane isomerization by catalysis—A method of industrial importance: An overview. *Cogent Chem.* **2018**, *4*, 1514686. [CrossRef]
42. Morris, R.E.; Nachtigall, P. *Zeolites in Catalysis: Properties and Applications*; Royal Society of Chemistry: London, UK, 2017.
43. Primo, A.; Garcia, H. Zeolites as catalysts in oil refining. *Chem. Soc. Rev.* **2014**, *43*, 7548–7561. [CrossRef]
44. Gao, S.; Wu, Z. Advances in the One- Dimensional Pore Zeolite for Hydroisomerization. *J. Petrochem. Univ.* **2023**, *36*, 51. [CrossRef]
45. Zhang, L.; Bai, X.; Fu, W.; Yang, X.; Sun, F.; He, L.; Tang, T. Superior activity and isomerization selectivity in n-dodecane hydroisomerization over Ni clusters on ZSM-22 zeolite with structural defects. *Fuel* **2023**, *332*, 126204. [CrossRef]
46. Zhang, Y.; Liu, D.; Lou, B.; Yu, R.; Men, Z.; Li, M.; Li, Z. Hydroisomerization of n-decane over micro/mesoporous Pt-containing bifunctional catalysts: Effects of the MCM-41 incorporation with Y zeolite. *Fuel* **2018**, *226*, 204–212. [CrossRef]
47. Csicsery, S.M. Shape-selective catalysis in zeolites. *Zeolites* **1984**, *4*, 202–213. [CrossRef]
48. Marcilly, C.R. Where and how shape selectivity of molecular sieves operates in refining and petrochemistry catalytic processes. *Top. Catal.* **2000**, *13*, 357–366. [CrossRef]
49. Degnan Jr, T.F. The implications of the fundamentals of shape selectivity for the development of catalysts for the petroleum and petrochemical industries. *J. Catal.* **2003**, *216*, 32–46. [CrossRef]
50. Han, Y.; Yuan, J.; Xing, M.; Cao, J.; Chen, Z.; Zhang, L.; Tao, Z.; Liu, Z.; Zheng, A.; Wen, X. Shape selectivity of zeolite for hydroisomerization of long-chain alkanes. *New J. Chem.* **2023**, *47*, 1401–1412. [CrossRef]
51. Wang, M.; Han, Y.; Liu, S.; Liu, Z.; An, D.; Zhang, Z.; Cheng, K.; Zhang, Q.; Wang, Y. Pore-mouth catalysis boosting the formation of iso-paraffins from syngas over bifunctional catalysts. *Chin. J. Catal.* **2021**, *42*, 2197–2205. [CrossRef]
52. Brito, L.; Pirngruber, G.D.; Perez-Pellitero, J.; Guillon, E.; Albrieux, F.; Martens, J.A. Shape selectivity effects in the hydroconversion of perhydrophenanthrene over bifunctional catalysts. *Catal. Sci. Technol.* **2021**, *11*, 7667–7682. [CrossRef]
53. Guo, Z.; Li, X.; Hu, S.; Ye, G.; Zhou, X.; Coppens, M.O. Understanding the role of internal diffusion barriers in Pt/Beta zeolite catalyzed isomerization of *n*-heptane. *Angew. Chem.* **2020**, *132*, 1564–1567. [CrossRef]
54. Chen, N.; Lucki, S.; Mower, E. Cage effect on product distribution from cracking over crystalline aluminosilicate zeolites. *J. Catal.* **1969**, *13*, 329–332. [CrossRef]
55. Kärger, J.; Ruthven, D.M.; Valiullin, R. Diffusion in nanopores: Inspecting the grounds. *Adsorption* **2021**, *27*, 267–281. [CrossRef]
56. Derouane, E.G. Shape selectivity in catalysis by zeolites: The nest effect. *J. Catal.* **1986**, *100*, 541–544. [CrossRef]
57. Romero, D.; Rohling, R.; Meng, L.; Rigutto, M.; Hensen, E.J. Shape selectivity in linear paraffins hydroconversion in 10-membered-ring pore zeolites. *J. Catal.* **2021**, *394*, 284–298. [CrossRef]
58. Yu, Q.; Huang, Z.; Sun, H.; Li, L.; Zhu, X.; Ren, S.; Shen, B. Investigation on *n*-Alkane Hydroisomerization, a Comparison of IM-5 to ZSM-5 Zeolites. *Ind. Eng. Chem. Res.* **2018**, *57*, 14448–14459. [CrossRef]
59. Mehla, S.; Krishnamurthy, K.; Viswanathan, B.; John, M.; Niwate, Y.; Kumar, K.; Pai, S.M.; Newalkar, B. *n*-Hexadecane hydroisomerization over Pt/ZSM-12: Role of Si/Al ratio on product distribution. *J. Porous Mater.* **2013**, *20*, 1023–1029. [CrossRef]
60. Araujo, A.S.; Silva, A.O.; Souza, M.J.; Coutinho, A.C.; Aquino, J.M.; Moura, J.A.; Pedrosa, A.M. Crystallization of ZSM-12 zeolite with different Si/Al ratio. *Adsorption* **2005**, *11*, 159–165. [CrossRef]
61. Li, S.; Liutkova, A.; Kosinov, N.; Hensen, E.J. Zeolite Nanocrystals (MOR, EU-1, and ZSM-12) Synthesized Using a Versatile Diquaternary Ammonium Template as Robust Catalysts. *ACS Appl. Nano Mater.* **2022**, *5*, 16862–16871. [CrossRef]
62. Gopal, S.; Yoo, K.; Smirniotis, P.G. Synthesis of Al-rich ZSM-12 using TEAOH as template. *Microporous Mesoporous Mater.* **2001**, *49*, 149–156. [CrossRef]
63. Mehla, S.; Krishnamurthy, K.; Viswanathan, B.; John, M.; Niwate, Y.; Kumar, S.K.; Pai, S.M.; Newalkar, B.L. *n*-Hexadecane hydroisomerization over BTMACl/TEABr/MTEABr templated ZSM-12. *Microporous Mesoporous Mater.* **2013**, *177*, 120–126. [CrossRef]
64. Masoumifard, N.; Kaliaguine, S.; Kleitz, F. Synergy between structure direction and alkalinity toward fast crystallization, controlled morphology and high phase purity of ZSM-12 zeolite. *Microporous Mesoporous Mater.* **2016**, *227*, 258–271. [CrossRef]
65. Li, S.; Mezari, B.; Wu, H.; Kosinov, N.; Hensen, E.J. ZSM-12 nanocrystals with tunable acidity directed by rigid diquats: Synthesis and catalytic applications. *Fuel* **2023**, *333*, 126363. [CrossRef]

66. Silva, B.J.; de Sousa, L.V.; Quintela, P.H.; Júnior, N.R.A.; Alencar, S.L.; Maciel, P.A.; Santos, J.R.; Sarmento, L.R.; Meneghetti, S.M.; Silva, A. Preparation of ZSM-22 zeolite with hierarchical pore structure. *Mater. Lett.* **2018**, *218*, 119–122. [CrossRef]
67. Verboekend, D.; Chabaneix, A.M.; Thomas, K.; Gilson, J.-P.; Pérez-Ramírez, J. Mesoporous ZSM-22 zeolite obtained by desilication: Peculiarities associated with crystal morphology and aluminium distribution. *CrystEngComm* **2011**, *13*, 3408–3416. [CrossRef]
68. Niu, P.; Xi, H.; Ren, J.; Lin, M.; Wang, Q.; Jia, L.; Hou, B.; Li, D. High selectivity for *n*-dodecane hydroisomerization over highly siliceous ZSM-22 with low Pt loading. *Catal. Sci. Technol.* **2017**, *7*, 5055–5068. [CrossRef]
69. Wang, Y.; Yu, J.; Yang, F.; Zhao, Y.; Zhuang, J.; Lu, X.; Zhu, X.; Zhu, K. Synthesis of ZSM-22 with Enhanced Acidity Using Alcoholamine as a Structure-Directing Agent to Promote the Hydroisomerization of *n*-Heptane. *Ind. Eng. Chem. Res.* **2023**, *62*, 10012–10023. [CrossRef]
70. Wang, B.; Tian, Z.; Li, P.; Wang, L.; Xu, Y.; Qu, W.; He, Y.; Ma, H.; Xu, Z.; Lin, L. A novel approach to synthesize ZSM-23 zeolite involving *N*,*N*-dimethylformamide. *Microporous Mesoporous Mater.* **2010**, *134*, 203–209. [CrossRef]
71. Molino, A.; Łukaszuk, K.; Rojo-Gama, D.; Lillerud, K.P.; Olsbye, U.; Bordiga, S.; Svelle, S.; Beato, P. Conversion of methanol to hydrocarbons over zeolite ZSM-23 (MTT): Exceptional effects of particle size on catalyst lifetime. *Chem. Comm.* **2017**, *53*, 6816–6819. [CrossRef]
72. Chen, Y.; Li, C.; Chen, X.; Liu, Y.; Liang, C. Synthesis of ZSM-23 zeolite with dual structure directing agents for hydroisomerization of *n*-hexadecane. *Microporous Mesoporous Mater.* **2018**, *268*, 216–224. [CrossRef]
73. Ahmed, M.H.; Muraza, O.; Yoshioka, M.; Yokoi, T. Effect of multi-step desilication and dealumination treatments on the performance of hierarchical EU-1 zeolite for converting methanol to olefins. *Microporous Mesoporous Mater.* **2017**, *241*, 79–88. [CrossRef]
74. Du, Y.; Feng, B.; Jiang, Y.; Yuan, L.; Huang, K.; Li, J. Solvent-Free Synthesis and n-Hexadecane Hydroisomerization Performance of SAPO-11 Catalyst. *Eur. J. Inorg. Chem.* **2018**, *2018*, 2599–2606. [CrossRef]
75. Zhang, Y.; Wang, W.; Jiang, X.; Su, X.; Kikhtyanin, O.; Wu, W. Hydroisomerization of *n*-hexadecane over a Pd–Ni_2P/SAPO-31 bifunctional catalyst: Synergistic effects of bimetallic active sites. *Catal. Sci. Technol.* **2018**, *8*, 817–828. [CrossRef]
76. Bai, X.; Wei, X.; Liu, Y.; Wu, W. Effect of dealumination of citric acid-modified Hβ molecular sieve on hydroisomerization performance of *n*-Hexadecane. In Proceedings of the IOP Conference Series: Materials Science and Engineering, The 6th Annual International Conference on Material Science and Environmental Engineering, Chongqing, China, 23–25 November 2018; p. 012040.
77. Bai, X.; Wei, X.; Liu, Y.; Wu, W. Hydroisomerization of n-hexadecane over Hβ molecular sieve loading palladium bifunctional catalyst: Effect of SiO_2/Al_2O_3 molar ratios. In Proceedings of the IOP Conference Series: Materials Science and Engineering, The 2nd International Workshop on Materials Science and Mechanical Engineering (IWMSME2018), Qingdao, China, 26–28 October 2018; p. 012042.
78. Smirniotis, P.G.; Ruckenstein, E. Comparison of the Performance of ZSM-5,.beta. Zeolite, Y, USY, and Their Composites in the Catalytic Cracking of *n*-Octane, 2,2,4-Trimethylpentane, and 1-Octene. *Ind. Eng. Chem. Res.* **1994**, *33*, 800–813. [CrossRef]
79. Zhang, J.; Maximov, A.; Bai, X.; Wang, W.; Xiao, L.; Lin, H.; Wu, W. Shape selectivity in hydroisomerization of *n*-Hexadecane over Pd supported on zeolites: ZSM-22, ZSM-12 and Beta. *Russ. J. Appl. Chem.* **2020**, *93*, 1427–1437. [CrossRef]
80. Zhang, M.; Chen, Y.; Wang, L.; Zhang, Q.; Tsang, C.-W.; Liang, C. Shape selectivity in hydroisomerization of hexadecane over Pt supported on 10-ring zeolites: ZSM-22, ZSM-23, ZSM-35, and ZSM-48. *Ind. Eng. Chem. Res.* **2016**, *55*, 6069–6078. [CrossRef]
81. Liu, Y.; Pinnavaia, T.J. Aluminosilicate nanoparticles for catalytic hydrocarbon cracking. *J. Am. Chem. Soc.* **2003**, *125*, 2376–2377. [CrossRef] [PubMed]
82. Karlsson, A.; Stoecker, M.; Schmidt, R. Composites of micro-and mesoporous materials: Simultaneous syntheses of MFI/MCM-41 like phases by a mixed template approach. *Microporous Mesoporous Mater.* **1999**, *27*, 181–192. [CrossRef]
83. Cheng, K.; van der Wal, L.I.; Yoshida, H.; Oenema, J.; Harmel, J.; Zhang, Z.; Sunley, G.; Zečević, J.; de Jong, K.P. Impact of the spatial organization of bifunctional metal–zeolite catalysts on the hydroisomerization of light alkanes. *Angew. Chem.* **2020**, *132*, 3620–3628. [CrossRef]
84. Chen, Z.; Liu, S.; Wang, H.; Ning, Q.; Zhang, H.; Yun, Y.; Ren, J.; Li, Y.-W. Synthesis and characterization of bundle-shaped ZSM-22 zeolite via the oriented fusion of nanorods and its enhanced isomerization performance. *J. Catal.* **2018**, *361*, 177–185. [CrossRef]
85. Morávková, J.; Pilař, R.; Bortnovsky, O.; Kaucký, D.; Vondrová, A.; Rathousky, J.; Sádovská, G.; Sazama, P. The effect of the nanoscale intimacy of platinum and acid centres on the hydroisomerization of short-chain alkanes. *Appl. Catal. A Gen.* **2022**, *634*, 118535. [CrossRef]
86. Ye, G.; Sun, Y.; Guo, Z.; Zhu, K.; Liu, H.; Zhou, X.; Coppens, M.-O. Effects of zeolite particle size and internal grain boundaries on Pt/Beta catalyzed isomerization of *n*-pentane. *J. Catal.* **2018**, *360*, 152–159. [CrossRef]
87. Wang, W.; Liu, C.-J.; Wu, W. Bifunctional catalysts for the hydroisomerization of *n*-alkanes: The effects of metal–acid balance and textural structure. *Catal. Sci. Technol.* **2019**, *9*, 4162–4187. [CrossRef]
88. Wang, Y.; Tao, Z.; Wu, B.; Xu, J.; Huo, C.; Li, K.; Chen, H.; Yang, Y.; Li, Y. Effect of metal precursors on the performance of Pt/ZSM-22 catalysts for *n*-hexadecane hydroisomerization. *J. Catal.* **2015**, *322*, 1–13. [CrossRef]
89. Geng, L.; Gong, J.; Qiao, G.; Ye, S.; Zheng, J.; Zhang, N.; Chen, B. Effect of metal precursors on the performance of Pt/SAPO-11 catalysts for *n*-dodecane hydroisomerization. *ACS Omega* **2019**, *4*, 12598–12605. [CrossRef] [PubMed]
90. Chen, H.; Yi, F.; Ma, C.; Gao, X.; Liu, S.; Tao, Z.; Wu, B.; Xiang, H.; Yang, Y.; Li, Y.-W. Hydroisomerization of *n*-heptane on a new kind of bifunctional catalysts with palladium nanoparticles encapsulating inside zeolites. *Fuel* **2020**, *268*, 117241. [CrossRef]

91. Guisnet, M. "Ideal" bifunctional catalysis over Pt-acid zeolites. *Catal. Today* **2013**, *218*, 123–134. [CrossRef]
92. Wang, Y.; Tao, Z.; Wu, B.; Huimin, C.; Xu, J.; Yang, Y.; Li, Y. Shape-controlled synthesis of Pt particles and their catalytic performances in the n-hexadecane hydroconversion. *Catal. Today* **2016**, *259*, 331–339. [CrossRef]
93. Roy, S.; Bouchy, C.; Pham-Huu, C.; Crouzet, C.; Ledoux, M.J. Slurry isomerization of *n*-hexadecane over MoO_3-carbon-modified, Pt/β-zeolite, Pt/ZSM-22 and Pt/SAPO-11 catalysts at medium pressure. In *Studies in Surface Science and Catalysis*; Corma, A., Melo, F.V., Mendiorozm, S., Fierro, J.L.G., Eds.; Elsevier: Amsterdam, The Netherlands, 2000; Volume 130, pp. 2423–2428.
94. Fedyna, M.; Żak, A.; Jaroszewska, K.; Mokrzycki, J.; Trawczyński, J. Composite of Pt/AlSBA-15+ zeolite catalyst for the hydroisomerization of *n*-hexadecane: The effect of platinum precursor. *Microporous Mesoporous Mater.* **2020**, *305*, 110366. [CrossRef]
95. Chen, Y.; Meng, J.; Bai, D.; Li, C.; Chen, X.; Liang, C. Effect of Extra-Framework Fe Species in Pt/Fe/ZSM-23 Catalysts on Hydroisomerization Performance of *n*-Hexadecane. *Ind. Eng. Chem. Res.* **2021**, *61*, 279–286. [CrossRef]
96. Song, C.Y.; Meng, J.P.; Chuang, L.I.; Zeyaodong, P.; Liang, C.H. Synthesis of ZSM-22/ZSM-23 intergrowth zeolite as the catalyst support for hydroisomerization of *n*-hexadecane. *J. Fuel Chem. Technol.* **2021**, *49*, 712–725. [CrossRef]
97. Zhang, M.; Li, C.; Chen, X.; Chen, Y.; Liang, C. Hierarchical ZSM-48-supported nickel catalysts with enhanced hydroisomerization performance of hexadecane. *Ind. Eng. Chem. Res.* **2019**, *58*, 19855–19861. [CrossRef]
98. Zhang, M.; Wang, L.; Chen, Y.; Zhang, Q.; Liang, C. Creating mesopores in ZSM-48 zeolite by alkali treatment: Enhanced catalyst for hydroisomerization of hexadecane. *J. Energy Chem.* **2016**, *25*, 539–544. [CrossRef]
99. Pimerzin, A.A.; Roganov, A.A.; Verevkin, S.P.; Konnova, M.E.; Pilshchikov, V.A.; Pimerzin, A.A. Bifunctional catalysts with noble metals on composite Al_2O_3-SAPO-11 carrier and their comparison with CoMoS one in n-hexadecane hydroisomerization. *Catal. Today* **2019**, *329*, 71–81. [CrossRef]
100. Zhao, X.; Xu, J.; Deng, F. Solid-state NMR for metal-containing zeolites: From active sites to reaction mechanism. *Front. Chem. Sci. Eng.* **2020**, *14*, 159–187. [CrossRef]
101. Schulman, E.; Wu, W.; Liu, D. Two-dimensional zeolite materials: Structural and acidity properties. *Materials* **2020**, *13*, 1822. [CrossRef]
102. Almutairi, S.M.; Mezari, B.; Filonenko, G.A.; Magusin, P.C.; Rigutto, M.S.; Pidko, E.A.; Hensen, E.J. Influence of extraframework aluminum on the brønsted acidity and catalytic reactivity of faujasite zeolite. *ChemCatChem* **2013**, *5*, 452–466. [CrossRef]
103. Izan, S.; Triwahyono, S.; Jalil, A.; Majid, Z.; Fatah, N.; Hamid, M.; Ibrahim, M. Additional Lewis acid sites of protonated fibrous silica@BEA zeolite (HSi@BEA) improving the generation of protonic acid sites in the isomerization of C_6 alkane and cycloalkanes. *Appl. Catal. A Gen.* **2019**, *570*, 228–237. [CrossRef]
104. Vogt, E.T.; Weckhuysen, B.M. Fluid catalytic cracking: Recent developments on the grand old lady of zeolite catalysis. *Chem. Soc. Rev.* **2015**, *44*, 7342–7370. [CrossRef]
105. Ennaert, T.; Van Aelst, J.; Dijkmans, J.; De Clercq, R.; Schutyser, W.; Dusselier, M.; Verboekend, D.; Sels, B.F. Potential and challenges of zeolite chemistry in the catalytic conversion of biomass. *Chem. Soc. Rev.* **2016**, *45*, 584–611. [CrossRef]
106. Dzhikiya, O.; Smolikov, M.; Belopukhov, E.; Yablokova, S.; Doronin, A.; Gulyaeva, T.; Muromtsev, I.; Belyi, A. A study of fluorine-containing catalysts based on MOR and BEA zeolites in isomerization of *n*-hexane. In Proceedings of the AIP Conference Proceedings, Oil and Gas Engineering (OGE-2020), Omsk, Russia, 26–29 February 2020.
107. Sun, J.; Mu, C.; Guo, D.; Zhao, Y.; Wang, S.; Ma, X. Effects of intimacy between acid and metal sites on the isomerization of n-C16 at the large/minor nanoscale and atomic scale. *ACS Catal.* **2022**, *12*, 4092–4102. [CrossRef]
108. Harmel, J.; van der Wal, L.; Zečević, J.; de Jongh, P.; de Jong, K.P. Metal-Acid Bifunctional Catalysts for Hydro-Isomerization of Alkanes: Impact of Intimacy for Mesoporous Solid Acids. In Proceedings of the 2019 North American Catalysis Society Meeting, Chicago, IL, USA, 23–28 June 2019.
109. Chen, Y.; Li, C.; Chen, X.; Liu, Y.; Tsang, C.-W.; Liang, C. Synthesis and characterization of iron-substituted ZSM-23 zeolite catalysts with highly selective hydroisomerization of *n*-hexadecane. *Ind. Eng. Chem. Res.* **2018**, *57*, 13721–13730. [CrossRef]
110. Blasco, T.; Chica, A.; Corma, A.; Murphy, W.; Agúndez-Rodríguez, J.; Pérez-Pariente, J. Changing the Si distribution in SAPO-11 by synthesis with surfactants improves the hydroisomerization/dewaxing properties. *J. Catal.* **2006**, *242*, 153–161. [CrossRef]
111. Gopal, S.; Smirniotis, P.G. Factors affecting isomer yield for n-heptane hydroisomerization over as-synthesized and dealuminated zeolite catalysts loaded with platinum. *J. Catal.* **2004**, *225*, 278–287. [CrossRef]
112. Yang, X.; Zhao, W.; Liu, L.; Niu, X.; Wang, Q. Tuning the Structure and Acidity of Pt/Hierarchical SSZ-32 Catalysts to Boost the Selective Hydroisomerization of n-Hexadecane. *Catalysts* **2023**, *13*, 702. [CrossRef]
113. Li, T.; Wang, W.; Feng, Z.; Bai, X.; Su, X.; Yang, L.; Jia, G.; Guo, C.; Wu, W. The hydroisomerization of n-hexane over highly selective Pd/ZSM-22 bifunctional catalysts: The improvements of metal-acid balance by room temperature electron reduction method. *Fuel* **2020**, *272*, 117717. [CrossRef]
114. Wei, C.; Zhang, G.; Zhao, L.; Gao, J.; Xu, C. Effect of metal–acid balance and textual modifications on hydroisomerization catalysts for *n*-alkanes with different chain length: A mini-review. *Fuel* **2022**, *315*, 122809. [CrossRef]
115. Batalha, N.; Pinard, L.; Bouchy, C.; Guillon, E.; Guisnet, M. n-Hexadecane hydroisomerization over Pt-HBEA catalysts. Quantification and effect of the intimacy between metal and protonic sites. *J. Catal.* **2013**, *307*, 122–131. [CrossRef]
116. Parmar, S.; Pant, K.K.; John, M.; Kumar, K.; Pai, S.M.; Gupta, S.; Newalkar, B.L. Hydroisomerization of n-hexadecane over Brønsted acid site tailored Pt/ZSM-12. *J. Porous Mater.* **2014**, *21*, 849–857. [CrossRef]

117. Lee, S.-W.; Ihm, S.-K. Characteristics of magnesium-promoted Pt/ZSM-23 catalyst for the hydroisomerization of *n*-hexadecane. *Ind. Eng. Chem. Res.* **2013**, *52*, 15359–15365. [CrossRef]
118. Liu, S.; Ren, J.; Zhu, S.; Zhang, H.; Lv, E.; Xu, J.; Li, Y.-W. Synthesis and characterization of the Fe-substituted ZSM-22 zeolite catalyst with high n-dodecane isomerization performance. *J. Catal.* **2015**, *330*, 485–496. [CrossRef]
119. Batalha, N.; Morisset, S.; Pinard, L.; Maupin, I.; Lemberton, J.; Lemos, F.; Pouilloux, Y. BEA zeolite nanocrystals dispersed over alumina for *n*-hexadecane hydroisomerization. *Microporous Mesoporous Mater.* **2013**, *166*, 161–166. [CrossRef]
120. Parmar, S.; Pant, K.K.; John, M.; Kumar, K.; Pai, S.M.; Newalkar, B.L. Hydroisomerization of n-hexadecane over Pt/ZSM-22 framework: Effect of divalent cation exchange. *J. Mol. Catal. A Chem.* **2015**, *404*, 47–56. [CrossRef]
121. Liu, L.; Zhang, M.; Wang, L.; Zhang, X.; Li, G. Modulating acid site distribution in MTT channels for controllable hydroisomerization of long-chain *n*-alkanes. *Fuel Process. Technol.* **2023**, *241*, 107605. [CrossRef]
122. Zhang, M.; Li, C.; Chen, Y.; Tsang, C.-W.; Zhang, Q.; Liang, C. Hydroisomerization of hexadecane over platinum supported on EU-1/ZSM-48 intergrowth zeolite catalysts. *Catal. Sci. Technol.* **2016**, *6*, 8016–8023. [CrossRef]
123. Wang, D.; Liu, J.; Cheng, X.; Kang, X.; Wu, A.; Tian, C.; Fu, H. Trace Pt Clusters Dispersed on SAPO-11 Promoting the Synergy of Metal Sites with Acid Sites for High-Effective Hydroisomerization of *n*-Alkanes. *Small Methods* **2019**, *3*, 1800510. [CrossRef]
124. Guo, C.; Wang, W.; Zhang, Y.; Lin, H.; Jia, G.; Li, T.; Xin, Q.; Bai, X.; Wu, W. Influences of the metal-acid proximity of Pd-SAPO-31 bifunctional catalysts for *n*-hexadecane hydroisomerization. *Fuel Process. Technol.* **2021**, *214*, 106717. [CrossRef]
125. Wei, X.; Kikhtyanin, O.; Parmon, V.; Wu, W.; Bai, X.; Zhang, J.; Xiao, L.; Su, X.; Zhang, Y. Synergetic effect between the metal and acid sites of Pd/SAPO-41 bifunctional catalysts in n-hexadecane hydroisomerization. *J. Porous Mater.* **2018**, *25*, 235–247. [CrossRef]
126. Jia, G.; Guo, C.; Wang, W.; Bai, X.; Wei, X.; Su, X.; Li, T.; Xiao, L.; Wu, W. The synergic effects of highly selective bimetallic Pt-Pd/SAPO-41 catalysts for the *n*-hexadecane hydroisomerization. *Front. Chem. Sci. Eng.* **2021**, *15*, 1111–1124. [CrossRef]
127. Wu, Q.; Jia, G.; Zhang, Y.; Liu, Z.; Li, X.; Wang, W.; Wu, W. Bifunctional catalysts based on hierarchical SAPO-41 nanosheet for Highly-efficient hydroisomerization of n-Hexadecane. *Fuel* **2023**, *352*, 129066. [CrossRef]
128. Mendes, P.S.; Mota, F.M.; Silva, J.M.; Ribeiro, M.F.; Daudin, A.; Bouchy, C. A systematic study on mixtures of Pt/zeolite as hydroisomerization catalysts. *Catal. Sci. Technol.* **2017**, *7*, 1095–1107. [CrossRef]
129. Bauer, F.; Ficht, K.; Bertmer, M.; Einicke, W.-D.; Kuchling, T.; Gläser, R. Hydroisomerization of long-chain paraffins over nano-sized bimetallic Pt–Pd/H-beta catalysts. *Catal. Sci. Technol.* **2014**, *4*, 4045–4054. [CrossRef]
130. Vinogradov, N.; Rubtsova, M.; Glotov, A.; Tochilin, N.; Vinokurov, V.; Pimerzin, A. Hydroconversion of n-Hexadecane on Zeolite-Containing Sulfide-Based Catalysts: Influence of Nitrogen Impurity in the Feedstock on the Hydroisomerization Selectivity. *Pet. Chem.* **2021**, *61*, 739–747. [CrossRef]
131. Jaroszewska, K.; Fedyna, M.; Trawczyński, J. Hydroisomerization of long-chain *n*-alkanes over Pt/AlSBA-15+ zeolite bimodal catalysts. *Appl. Catal. B Environ.* **2019**, *255*, 117756. [CrossRef]
132. Bogomolova, T.; Smirnova, M.Y.; Klimov, O.; Noskov, A. Studying the Hydroisomerization of Diesel Fractions with Different Concentrations of Nitrogen-Containing Compounds on Bifunctional Catalysts Based on ZSM-23 and Non-Noble Metals. *Catal. Ind.* **2023**, *15*, 182–189. [CrossRef]
133. Chen, N.; Degnan, T.; Lutner, J.; Pelrine, B. The deactivation of ZSM-5 in catalytic dewaxing. In *Studies in Surface Science and Catalysis*; Elsevier: Amsterdam, The Netherlands, 1991; Volume 68, pp. 773–782.
134. Galperin, L. Hydroisomerization of N-decane in the presence of sulfur and nitrogen compounds. *Appl. Catal. A Gen.* **2001**, *209*, 257–268. [CrossRef]
135. Lee, S.-W.; Ihm, S.-K. Hydroisomerization and hydrocracking over platinum loaded ZSM-23 catalysts in the presence of sulfur and nitrogen compounds for the dewaxing of diesel fuel. *Fuel* **2014**, *134*, 237–243. [CrossRef]
136. Pimerzin, A.; Savinov, A.; Vutolkina, A.; Makova, A.; Glotov, A.; Vinokurov, V.; Pimerzin, A. Transition metal sulfides-and noble metal-based catalysts for N-hexadecane hydroisomerization: A study of poisons tolerance. *Catalysts* **2020**, *10*, 594. [CrossRef]
137. Iskenderova, A. Mechanism of Catalytic Isomerization-Disproportionation Processing of Straight-Run Gasoline. *Azerbaijan Chem. J.* **2022**, *2*, 28–33. [CrossRef]
138. Sun, J.; Yu, Y.; Mu, C.; Guo, X.; Zhao, Y.; Wang, S.; Ma, X. The gradient fabrication and optimization of metal-acid bifunctional catalysts for the hydrogenation of n-C16 to produce bio-jet fuel component. *Fuel* **2023**, *353*, 129229. [CrossRef]
139. Pham, T.N.; Nguyen, V.; Wang, B.; White, J.L.; Crossley, S. Quantifying the influence of water on the mobility of aluminum species and their effects on alkane cracking in zeolites. *ACS Catal.* **2021**, *11*, 6982–6994. [CrossRef]
140. Yan, T. The promotional effect of water in hydrocracking. *J. Catal.* **1972**, *25*, 204–211. [CrossRef]
141. Brosius, R.; Kooyman, P.J.; Fletcher, J.C. Selective formation of linear alkanes from n-hexadecane primary hydrocracking in shape-selective MFI zeolites by competitive adsorption of water. *ACS Catal.* **2016**, *6*, 7710–7715. [CrossRef]
142. Guisnet, M.; Magnoux, P. Coking and deactivation of zeolites: Influence of the pore structure. *Appl. Catal.* **1989**, *54*, 1–27. [CrossRef]
143. Guisnet, M. "Coke" molecules trapped in the micropores of zeolites as active species in hydrocarbon transformations. *J. Mol. Catal. A Chem.* **2002**, *182*, 367–382. [CrossRef]
144. Sun, Y.; Wei, L.; Zhang, Z.; Zhang, H.; Li, Y. Coke formation over zeolite catalysts in light alkanes aromatization and anti-carbon-deposition strategies and perspectives: A review. *Energy Fuel* **2023**, *37*, 1657–1677. [CrossRef]

145. Guisnet, M.; Magnoux, P. Deactivation of zeolites by coking. Prevention of deactivation and regeneration. In *Zeolite Microporous Solids: Synthesis, Structure, and Reactivity*; Springer: Dordrecht, The Netherlands, 1992; pp. 457–474.
146. Nazarova, G.Y.; Ivashkina, E.N.; Ivanchina, E.D.; Vosmerikov, A.V.; Vosmerikova, L.N.; Antonov, A.V. A model of catalytic cracking: Product distribution and catalyst deactivation depending on saturates, aromatics and resins content in feed. *Catalysts* **2021**, *11*, 701. [CrossRef]
147. Muhammad, I.; Makwashi, N.; Ahmed, T.G.; Manos, G.; Zhao, D. A Mechanistic Model on Catalyst Deactivation by Coke Formation in a CSTR Reactor. *Processes* **2023**, *11*, 944. [CrossRef]
148. Guisnet, M.; Magnoux, P. Organic chemistry of coke formation. *Appl. Catal. A Gen.* **2001**, *212*, 83–96. [CrossRef]
149. Bauer, F.; Karge, H.G. Characterization of coke on zeolites. In *Characterization II*; Springer: Berlin/Heidelberg, Germany, 2006; pp. 249–364.
150. Guisnet, M.; Magnoux, P. Deactivation by coking of zeolite catalysts. Prevention of deactivation. Optimal conditions for regeneration. *Catal. Today* **1997**, *36*, 477–483. [CrossRef]
151. Guisnet, M.; Costa, L.; Ribeiro, F.R. Prevention of zeolite deactivation by coking. *J. Mol. Catal. A Chem.* **2009**, *305*, 69–83. [CrossRef]
152. Shehab, A. The Role of Carbon in the Catalytic Isomerisation-Cracking of n-Alkanes. Ph.D. Thesis, University of Sheffield, Sheffield, UK, 2018.
153. Brillis, A.A.; Manos, G. Coke formation during catalytic cracking of C8 aliphatic hydrocarbons over ultrastable Y zeolite. *Ind. Eng. Chem. Res.* **2003**, *42*, 2292–2298. [CrossRef]
154. Forzatti, P.; Lietti, L. Catalyst deactivation. *Catal. Today* **1999**, *52*, 165–181. [CrossRef]
155. Rombi, E.; Monaci, R.; Solinas, V. Kinetics of catalyst deactivation. An example: Methylnaphthalene transformation. *Catal. Today* **1999**, *52*, 321–330. [CrossRef]
156. Richardson, S.M.; Nagaishi, H.; Gray, M.R. Initial coke deposition on a NiMo/γ-Al_2O_3 bitumen hydroprocessing catalyst. *Ind. Eng. Chem. Res.* **1996**, *35*, 3940–3950. [CrossRef]
157. Muegge, B.; Massoth, F. Basic studies of deactivation of hydrotreating catalysts with anthracene. *Fuel Process. Technol.* **1991**, *29*, 19–30. [CrossRef]
158. Zhang, X.; Chodakowski, M.; Shaw, J.M. Impact of multiphase behavior on coke deposition in a commercial hydrotreating catalyst under sedimentation conditions. *Energy Fuel* **2005**, *19*, 1405–1411. [CrossRef]
159. Chen, S.; Manos, G. Study of coke and coke precursors during catalytic cracking of n-hexane and 1-hexene over ultrastable Y zeolite. *Catal. Lett.* **2004**, *96*, 195–200. [CrossRef]
160. Chen, S.; Manos, G. In situ thermogravimetric study of coke formation during catalytic cracking of normal hexane and 1-hexene over ultrastable Y zeolite. *J. Catal.* **2004**, *226*, 343–350. [CrossRef]
161. Holm, M.S.; Taarning, E.; Egeblad, K.; Christensen, C.H. Catalysis with hierarchical zeolites. *Catal. Today* **2011**, *168*, 3–16. [CrossRef]
162. Da Rocha, J.D.G.; Macuvele, D.L.P.; de Andrade, C.J.; Riella, H.G.; Padoin, N.; Soares, C. Advances and Environmental Aspects on the Synthesis of Hierarchical Zeolites Revisited: A State-of-the-Art Description. *J. Environ. Chem. Eng.* **2023**, *11*, 109397. [CrossRef]
163. Bornes, C.; Santos-Vieira, I.C.; Vieira, R.; Mafra, L.; Simões, M.M.; Rocha, J. Challenges and opportunities for zeolites in biomass upgrading: Impediments and future directions. *Catal. Today* **2023**, *419*, 114159. [CrossRef]
164. Hu, G.; Yang, J.; Duan, X.; Farnood, R.; Yang, C.; Yang, J.; Liu, W.; Liu, Q. Recent developments and challenges in zeolite-based composite photocatalysts for environmental applications. *Chem. Eng. J.* **2021**, *417*, 129209. [CrossRef]
165. Gosselink, R.W.; Sagala, S.L.; Meeldijk, J.D.; de Jongh, P.E.; de Jong, K.P. Alkaline treatment on commercially available aluminum rich mordenite. *Appl. Catal. A Gen.* **2010**, *382*, 65–72. [CrossRef]
166. Sazama, P.; Pastvova, J.; Kaucky, D.; Moravkova, J.; Rathousky, J.; Jakubec, I.; Sadovska, G. Does hierarchical structure affect the shape selectivity of zeolites? Example of transformation of *n*-hexane in hydroisomerization. *J. Catal.* **2018**, *364*, 262–270. [CrossRef]
167. Meng, J.; Cui, T.; Bai, D.; Li, C.; Chen, X.; Liang, C. Excellent catalytic performance over hierarchical ZSM-48 zeolite: Cooperative effects of enhanced mesoporosity and highly-accessible acidity. *Fuel* **2022**, *324*, 124589. [CrossRef]
168. Gackowski, M.; Tarach, K.; Podobiński, J.; Jarczewski, S.; Kuśtrowski, P.; Datka, J. Hierarchical zeolites Y obtained by desilication: Porosity, acidity and catalytic properties. *Microporous Mesoporous Mater.* **2018**, *263*, 282–288. [CrossRef]
169. Aumond, T.; Rousseau, J.; Pouilloux, Y.; Pinard, L.; Sachse, A. Synthesis of hierarchical zeolite templated carbons. *Carbon Trends* **2021**, *2*, 100014. [CrossRef]
170. Hu, B.; Zhang, Z.X.; Xie, W.L.; Liu, J.; Li, Y.; Zhang, W.M.; Fu, H.; Lu, Q. Advances on the fast pyrolysis of biomass for the selective preparation of phenolic compounds. *Fuel Process. Technol.* **2022**, *237*, 107465. [CrossRef]
171. Yue, Y.; Hu, Y.; Dong, P.; Li, X.; Liu, H.; Bao, J.; Wang, T.; Bi, X.; Zhu, H.; Yuan, P. Mesoscale depolymerization of natural rectorite mineral via a quasi-solid-phase approach for zeolite synthesis. *Chem. Eng. Sci.* **2020**, *220*, 115635. [CrossRef]
172. Imbachi-Gamba, C.F.; Villa, A. Statistical analysis of the influence of synthesis conditions on the properties of hierarchical zeolite Y. *Mater. Today Chem.* **2021**, *20*, 100442. [CrossRef]
173. Jermy, B.R.; Tanimu, A.; Siddiqui, M.A.; Qureshi, Z.S.; Aitani, A.; Akah, A.; Xu, Q.; AlHerz, M. Crude oil conversion to chemicals over green synthesized ZSM-5 zeolite. *Fuel Process. Technol.* **2023**, *241*, 107610. [CrossRef]
174. Ndlovu, N.Z.; Ameh, A.E.; Petrik, L.F.; Ojumu, T.V. Synthesis and characterisation of pure phase ZSM-5 and sodalite zeolites from coal fly ash. *Mater. Today Commun.* **2023**, *34*, 105436. [CrossRef]

175. Nguyen, D.K.; Dinh, V.P.; Nguyen, H.Q.; Hung, N.T. Zeolite ZSM-5 synthesized from natural silica sources and its applications: A critical review. *J. Chem. Technol. Biotechnol.* **2023**, *98*, 1339–1355. [CrossRef]
176. Demikhova, N.; Rubtsova, M.; Kireev, G.; Cherednichenko, K.; Vinokurov, V.; Glotov, A. Micro-mesoporous catalysts based on ZSM-5 zeolite synthesized from natural clay nanotubes: Preparation and application in the isomerization of C-8 aromatic fraction. *Chem. Eng. J.* **2023**, *453*, 139581. [CrossRef]
177. Stavitskaya, A.; Rubtsova, M.; Glotov, A.; Vinokurov, V.; Vutolkina, A.; Fakhrullin, R.; Lvov, Y. Architectural design of core–shell nanotube systems based on aluminosilicate clay. *Nanoscale Adv.* **2022**, *4*, 2823–2835. [CrossRef] [PubMed]
178. Glotov, A.; Levshakov, N.; Stavitskaya, A.; Artemova, M.; Gushchin, P.; Ivanov, E.; Vinokurov, V.; Lvov, Y. Templated self-assembly of ordered mesoporous silica on clay nanotubes. *Chem. Commun.* **2019**, *55*, 5507–5510. [CrossRef] [PubMed]
179. Glotov, A.; Vutolkina, A.; Pimerzin, A.; Nedolivko, V.; Zasypalov, G.; Stytsenko, V.; Karakhanov, E.; Vinokurov, V. Ruthenium catalysts templated on mesoporous MCM-41 type silica and natural clay nanotubes for hydrogenation of benzene to cyclohexane. *Catalysts* **2020**, *10*, 537. [CrossRef]
180. Glotov, A.; Vutolkina, A.; Pimerzin, A.; Vinokurov, V.; Lvov, Y. Clay nanotube-metal core/shell catalysts for hydroprocesses. *Chem. Soc. Rev.* **2021**, *50*, 9240–9277. [CrossRef]
181. Al-Jubouri, S.M.; Al-Batty, S.I.; Holmes, S.M. Using the ash of common water reeds as a silica source for producing high purity ZSM-5 zeolite microspheres. *Microporous Mesoporous Mater.* **2021**, *316*, 110953. [CrossRef]
182. Khoshbin, R.; Karimzadeh, R. The beneficial use of ultrasound in free template synthesis of nanostructured ZSM-5 zeolite from rice husk ash used in catalytic cracking of light naphtha: Effect of irradiation power. *Adv. Powder Technol.* **2017**, *28*, 973–982. [CrossRef]
183. Wang, Y.; Jia, H.; Chen, P.; Fang, X.; Du, T. Synthesis of La and Ce modified X zeolite from rice husk ash for carbon dioxide capture. *J. Mater. Res. Technol.* **2020**, *9*, 4368–4378. [CrossRef]
184. Flores, C.G.; Schneider, H.; Dornelles, J.S.; Gomes, L.B.; Marcilio, N.R.; Melo, P.J. Synthesis of potassium zeolite from rice husk ash as a silicon source. *Clean. Eng. Technol.* **2021**, *4*, 100201. [CrossRef]
185. Tran-Nguyen, P.L.; Ly, K.-P.; Thanh, L.H.V.; Angkawijaya, A.E.; Santoso, S.P.; Tsai, M.-L.; Ju, Y.-H. Facile synthesis of zeolite NaX using rice husk ash without pretreatment. *J. Taiwan Inst. Chem. Eng.* **2021**, *123*, 338–345. [CrossRef]
186. Masoumi, F.; Safari, S.; Khoshbin, R.; Karimzadeh, R. Utilization of agricultural waste (rice husk) in synthesis of TS-1 zeolite as a support for NiMo nanocatalyst employed in hydrodesulfurization of heavy oil. *Adv. Powder Technol.* **2023**, *34*, 104134. [CrossRef]
187. Lee, J.B.; Ahmed, I.; Lee, G.; Kim, T.-W.; Kim, C.-U.; Jhung, S.H. Synthesis of SSZ-13 zeolites using calcined rice husk as silica source for propylene production from ethylene and carbon dioxide adsorption. *J. Ind. Eng. Chem.* **2023**. [CrossRef]
188. Liu, H.; Yue, Y.; Shen, T.; Wang, W.; Li, T.; Bao, X. Transformation and crystallization behaviors of titanium species in synthesizing Ti-ZSM-5 zeolites from natural rectorite mineral. *Ind. Eng. Chem. Res.* **2019**, *58*, 11861–11870. [CrossRef]
189. Yue, Y.; Kang, Y.; Bai, Y.; Gu, L.; Liu, H.; Bao, J.; Wang, T.; Yuan, P.; Zhu, H.; Bai, Z. Seed-assisted, template-free synthesis of ZSM-5 zeolite from natural aluminosilicate minerals. *Appl. Clay Sci.* **2018**, *158*, 177–185. [CrossRef]
190. Servatan, M.; Ghadiri, M.; Yazdi, M.K.; Jouyandeh, M.; Mahmodi, G.; Samadi, A.; Zarrintaj, P.; Habibzadeh, S.; Ganjali, M.R.; Saeb, M.R. Synthesis of cost-effective hierarchical MFI-type mesoporous zeolite: Introducing diatomite as silica source. *Silicon* **2021**, *13*, 3461–3472. [CrossRef]
191. Asl, S.M.H.; Masomi, M.; Tajbakhsh, M. Hybrid adaptive neuro-fuzzy inference systems for forecasting benzene, toluene & m-xylene removal from aqueous solutions by HZSM-5 nano-zeolite synthesized from coal fly ash. *J. Clean. Prod.* **2020**, *258*, 120688. [CrossRef]
192. Rajakrishnamoorthy, P.; Karthikeyan, D.; Saravanan, C. Emission reduction technique applied in SI engines exhaust by using zsm5 zeolite as catalysts synthesized from coal fly ash. *Mater. Today Proc.* **2020**, *22*, 499–506. [CrossRef]
193. Song, C.-M.; Feng, Y.; Ma, L.-L. Characterization and hydroisomerization performance of SAPO-11 molecular sieves synthesized by dry gel conversion. *Microporous Mesoporous Mater.* **2012**, *147*, 205–211. [CrossRef]
194. Cai, R.; Sun, M.; Chen, Z.; Munoz, R.; O'Neill, C.; Beving, D.E.; Yan, Y. Ionothermal synthesis of oriented zeolite AEL films and their application as corrosion-resistant coatings. *Angew. Chem. Int. Ed.* **2008**, *47*, 525–528. [CrossRef] [PubMed]
195. Jin, Y.; Chen, X.; Sun, Q.; Sheng, N.; Liu, Y.; Bian, C.; Chen, F.; Meng, X.; Xiao, F.S. Solvent-Free Syntheses of Hierarchically Porous Aluminophosphate-Based Zeolites with AEL and AFI Structures. *Chem. A Eur. J.* **2014**, *20*, 17616–17623. [CrossRef] [PubMed]
196. Ren, L.; Wu, Q.; Yang, C.; Zhu, L.; Li, C.; Zhang, P.; Zhang, H.; Meng, X.; Xiao, F.-S. Solvent-free synthesis of zeolites from solid raw materials. *J. Am. Chem. Soc.* **2012**, *134*, 15173–15176. [CrossRef]
197. Zhang, H.; Wang, B.; Yan, W. The structure-directing role of heterologous seeds in the synthesis of zeolite. *Green Energy Environ.* **2023**. [CrossRef]
198. Ren, B.; Wang, J.; Zhou, Z.; Du, P.; Zhang, X. Regulation of the composition of metakaolin-based geopolymer: Effect of zeolite crystal seeds. *Case Stud. Constr. Mater.* **2023**, *19*, e02421. [CrossRef]
199. Kadja, G.T.; Azhari, N.J.; Mukti, R.R.; Khalil, M. A mechanistic investigation of sustainable solvent-free, seed-directed synthesis of ZSM-5 zeolites in the absence of an organic structure-directing agent. *ACS Omega* **2020**, *6*, 925–933. [CrossRef] [PubMed]
200. Shestakova, D.O.; Babina, K.A.; Sladkovskiy, D.A.; Parkhomchuk, E.V. Seed-assisted synthesis of hierarchical zeolite ZSM-5 in the absence of organic templates. *Mater. Chem. Phys.* **2022**, *288*, 126432. [CrossRef]
201. Bu, L.; Wang, Y.; Liu, W.; Chu, K.; Guo, N.; Huang, Y.; Qu, L.; Su, X.; Zhang, X.; Li, Y. Green synthesis of shaped nano-ZSM-5 toward more efficient methanol-to-hydrocarbon conversion. *Appl. Catal. A Gen.* **2023**, *665*, 119393. [CrossRef]

202. Nguyen, D.-K.; Dinh, V.-P.; Dang, N.; Khan, D.T.; Hung, N.T.; Tran, N.H.T. Effects of aging and hydrothermal treatment on the crystallization of ZSM-5 zeolite synthesis from bentonite. *RSC Adv.* **2023**, *13*, 20565–20574. [CrossRef]
203. Han, S.; Liu, Y.; Yin, C.; Jiang, N. Fast synthesis of submicron ZSM-5 zeolite from leached illite clay using a seed-assisted method. *Microporous Mesoporous Mater.* **2019**, *275*, 223–228. [CrossRef]
204. Jain, R.; Rimer, J.D. Seed-Assisted zeolite synthesis: The impact of seeding conditions and interzeolite transformations on crystal structure and morphology. *Microporous Mesoporous Mater.* **2020**, *300*, 110174. [CrossRef]
205. Chawla, A.; Jain, R.; Linares, N.; Martínez, J.G.; Rimer, J.D. Synthesis of Hierarchical Zeolite ZSM-11 Catalysts Via a Novel Organic-Free Route. In Proceedings of the 2019 North American Catalysis Society Meeting, Chicago, IL, USA, 23–28 June 2019.
206. Zhu, D.; Wang, L.; Cui, W.; Tan, J.; Tian, P.; Liu, Z. High-silica zeolite Y: Seed-assisted synthesis, characterization and catalytic properties. *Inorg. Chem. Front.* **2022**, *9*, 2213–2220. [CrossRef]
207. Velaga, B.; Peela, N.R. Seed-assisted and OSDA-free synthesis of H-mordenite zeolites for efficient production of 5-hydroxymethylfurfural from glucose. *Microporous Mesoporous Mater.* **2019**, *279*, 211–219. [CrossRef]
208. Deng, X.; Zhou, P.; Yan, X.; Xiong, R.; Kou, H.; Luo, W. Green synthesis of low-silica CHA zeolite without organic structural directing agents, fluoride media and seeds. *Microporous Mesoporous Mater.* **2021**, *310*, 110618. [CrossRef]
209. Meng, J.; Li, C.; Chen, X.; Song, C.; Liang, C. Seed-assisted synthesis of ZSM-48 zeolite with low SiO_2/Al_2O_3 ratio for n-hexadecane hydroisomerization. *Microporous Mesoporous Mater.* **2020**, *309*, 110565. [CrossRef]
210. Kamimura, Y.; Iyoki, K.; Elangovan, S.P.; Itabashi, K.; Shimojima, A.; Okubo, T. OSDA-free synthesis of MTW-type zeolite from sodium aluminosilicate gels with zeolite beta seeds. *Microporous Mesoporous Mater.* **2012**, *163*, 282–290. [CrossRef]
211. Kamimura, Y.; Itabashi, K.; Okubo, T. Seed-assisted, OSDA-free synthesis of MTW-type zeolite and "Green MTW" from sodium aluminosilicate gel systems. *Microporous Mesoporous Mater.* **2012**, *147*, 149–156. [CrossRef]
212. Muraza, O.; Abdul-lateef, A.; Tago, T.; Nandiyanto, A.B.; Konno, H.; Nakasaka, Y.; Yamani, Z.H.; Masuda, T. Microwave-assisted hydrothermal synthesis of submicron ZSM-22 zeolites and their applications in light olefin production. *Microporous Mesoporous Mater.* **2015**, *206*, 136–143. [CrossRef]
213. Sadeghpour, P.; Haghighi, M.; Ebrahimi, A. Ultrasound-assisted rapid hydrothermal design of efficient nanostructured MFI-Type aluminosilicate catalyst for methanol to propylene reaction. *Ultrason. Sonochem.* **2021**, *72*, 105416. [CrossRef] [PubMed]
214. Ramirez-Mendoza, H.; Valdez Lancinha Pereira, M.; Van Gerven, T.; Lutz, C.; Julian, I. Ultrasound-assisted preparation of Mo/ZSM-5 zeolite catalyst for non-oxidative methane dehydroaromatization. *Catalysts* **2021**, *11*, 313. [CrossRef]
215. Wang, B.; Wu, J.; Yuan, Z.-Y.; Li, N.; Xiang, S. Synthesis of MCM-22 zeolite by an ultrasonic-assisted aging procedure. *Ultrason. Sonochem.* **2008**, *15*, 334–338. [CrossRef]
216. Kumar, N.; Masloboischikova, O.; Kustov, L.; Heikkilä, T.; Salmi, T.; Murzin, D.Y. Synthesis of Pt modified ZSM-5 and beta zeolite catalysts: Influence of ultrasonic irradiation and preparation methods on physico-chemical and catalytic properties in pentane isomerization. *Ultrason. Sonochem.* **2007**, *14*, 122–130. [CrossRef]
217. Palanisamy, S.; Palanisamy, D.; Gul, M.; Kandasamy, K.; Gevert, B.S. Hydro-treating and Hydro-isomerisation of Sunflower Oil using Pt/SAPO-11: Influence of Templates in Ultrasonic Assisted with Hydrothermal Synthesis. *Bull. Chem. React. Eng. Catal.* **2021**, *16*, 120–135. [CrossRef]